Available online at www.sciencedirect.com

ScienceDirect

Current Opinion in Electrochemistry

Review Article

CO_2 electrolysis toward acetate: A review

Haoyuan Wang[1,2,a], Jing Xue[1,2,a], Chunxiao Liu[3], Zhaoyang Chen[3], Chengbo Li[3], Xu Li[3], Tingting Zheng[3], Qiu Jiang[1,3] and Chuan Xia[1,3,4]

Abstract

Storing renewable electricity from intermittent energy resources by turning waste CO_2 into versatile chemicals is promising for sustainable energy economy. In this process, multi-carbon products, especially acetate, are hard to achieve due to the high energy barrier and low selectivity for C−C coupling. Targeting acetate as a CO_2 electroreduction reactions (CO_2RR) end-product is perspective to reform the current acetate industry. Herein, we summarize the two major CO_2-to-acetate routes: the direct route via CO_2RR and the indirect one via CO reduction reaction (CORR). We firstly summarize reaction mechanisms for different routes; then discussed several categories of catalysts for acetate production via CO_2RR or CORR. We also correlate the theoretical calculations and experimental results to better understand the catalyst design principles. Finally, challenges and opportunities in current established processes are proposed. We aim to build a systematic understanding of current CO_2-to-acetate strategies and offer practical design guidelines for industrial CO_2-to-acetate production.

Addresses

[1] Yangtze Delta Region Institute (Huzhou), University of Electronic Science and Technology of China, Huzhou 313000, PR China
[2] Hefei National Laboratory for Physical Sciences at the Microscale, University of Science and Technology of China, Hefei, Anhui 230026, PR China
[3] School of Materials and Energy, University of Electronic Science and Technology of China, Chengdu 611731, PR China
[4] Research Center for Carbon-Neutral Environmental & Energy Technology, University of Electronic Science and Technology of China, Chengdu 611731, PR China

Corresponding authors: Xia Chuan (chuan.xia@uestc.edu.cn); Jiang Qiu (jiangqiu@uestc.edu.cn)
[a] Contributed equally to this work.

Current Opinion in Electrochemistry 2023, **39**:101253

This review comes from a themed issue on **Energy Transformation**

Edited by **Yung-Eun Sung** and **Dong Young Chung**

For a complete overview see the Issue and the Editorial

Available online 24 February 2023

https://doi.org/10.1016/j.coelec.2023.101253

Keywords

CO_2 electrolysis, Acetate, Catalysts, Reaction mechanisms, Selectivity.

Introduction

Since the industrial revolution, the consumption of fossil fuels has been increasing and has caused severe environmental problems due to the accumulated greenhouse gases, especially CO_2. The more frequent extreme weathers alert humans to change the current energy infrastructure and develop efficient carbon recycling techniques [1]. Replacing fossil fuels with renewable energy resources, including solar, wind, bio, and geothermal energy offers a sustainable solution to reduce the greenhouse effects [2,3]. However, those intermittent renewable energies are difficult to be integrated with the current power grids unless appropriate energy storage technologies are developed. Alternatively, CO_2 electroreduction reaction (CO_2RR) offers a potential pathway to store intermittent renewable electricity in the form of chemical energy and help to close the carbon cycle [4−6]. In the past few decades, tremendous efforts have been devoted to designing highly efficient electrocatalysts toward converting CO_2 into value-added chemicals. Among those, the energy efficiency toward C_1 products such as CO [7,8] and HCOOH [9,10] has hitherto approached commercialization, while efficiency and selectivity for multicarbon (C_{2+}) to date are still far from satisfactory.

Acetic acid (or acetate) is a crucial feedstock for many industrial processes. As an essential component in vinegar, global acetic acid production reaches more than ten million tons [11]. In addition, downstream products such as acetic anhydride and vinyl acetate play an important role in organic synthesis, plastic materials, medicine, and agriculture as bulk chemicals [12−14]. More importantly, recent research in biosynthesis showed that acetic acid could be converted to other value-added long-chain complex chemicals. For instance, *Escherichia coli* consumes acetate and converts it to succinate following an engineered metabolic path [15]. Similarly, other biological products, including glucose, fatty acids [16], acetyl-CoA [17], and 3-hydroxypropionic acid [18], can also be obtained from acetate. To date, the industrial production of acetic acid is dominated by the methanol carbonylation process, commercialized by BASF company in 1955 [19]. The process is energy-intensive and creates lots of harmful organics, and the recycling of precious rhodium-based

catalysts yields additional expenditure. Importantly, its equipment is prone to be corroded by iodide additives. On the contrary, the CO_2RR can run at or near room temperature and ambient pressure, and the intermittent production stream is more flexible compared with the traditional thermal process. Moreover, the decreasing price of renewable electricity is making the CO_2RR more cost-competitive as an energy-storage strategy [20]. Thus, it is appealing to explore the CO_2-to-acetate process by electrocatalysis. Although encouraging results have been achieved for the production of ethylene and ethanol using Cu-based catalysts [21—24], reports about CO_2 electrolysis toward acetic acid are relatively scarce. Cu is the only known metal that can effectively generate multicarbon (C_{2+}) products in the CO_2RR [25], whereas acetate is always presented as the byproduct of ethanol or ethylene production. On the current technical level, it is a daunting task to achieve both high selectivity and activity toward acetate formation via the direct CO_2 electrolysis route. In contrast, an indirect technological approach combining consecutive CO_2-to-CO and CO-to-acetate processes is a potential method for efficient acetate production, considering the well-established CO_2-to-CO process and the unique ability of CO electrolyzers to produce acetate selectively.

In this review, we take a broad and historical view of the electrocatalytic CO_2-to-acetate techniques from different aspects, including mechanistic study, catalyst optimization and electrolyzer design for both direct CO_2RR and indirect CO_2—CO-acetate pathways. For the direct CO_2RR, CO_2 activation and C—C bond formation are the two key mechanistic steps. Given that CO_2 is quite stable in the redox reaction [26], the as-designed CO_2RR catalysts are expected to show a low initial CO_2 activation energy [27]. In this regard, some state-of-the-art catalysts are presented, and current strategies to activate inert CO_2 molecules and facilitate C—C bond formation toward acetate are discussed. As a more favorable alternative, the indirect CO_2RR via CORR pathway undergoes deeper and further studies. The indirect pathway is commonly implemented by designing tandem electrodes or by decoupling the CO_2-to-CO and CO-to-acetate processes. As CO_2-to-CO process has been maturely exploited, here we put more emphases on the CORR to acetate. For CORR, the adsorbed *CO species are generally regarded as the key intermediate toward C_{2+} oxygenates [28,29]; hence, we specifically focus on the catalysts optimization strategies to tune the absorption energy on *CO. Along these lines, in this review, we systematically summarize the reported mechanisms of acetate formation via CO_2RR and CORR, respectively, to illustrate how to promote the formation of certain intermediates. We then discuss catalyst design strategies to break the Brönsted-Evans-Polanyi (BEP) relationship [30—32] for achieving higher acetate selectivity and efficiency. To make the review comprehensive, the investigations about non-catalyst factors associated with acetate formation are also included. Finally, we highlight the current drawbacks in the direct and indirect pathways and propose constructive solutions for future studies.

Direct CO_2RR toward acetate

State-of-the-art research of CO_2RR toward acetate

Efficient electrochemical reduction of CO_2 to C_{2+} products is of great importance, given that most of them are useful chemicals or fuels that can only be obtained from complicated and energy-consuming industrial synthesis [33]. In particular, the direct electroreduction of CO_2 toward acetate/acetic acid has attracted intensive interest since its production is otherwise achieved under high temperatures and through a multistep process from methane-derived syngas and successive carbonylation [34]. In addition, acetic acid has the potential to be further converted into long-chain products via synthetic biology to obtain products with higher energy density and market value [16]. However, due to the high barrier for C—C bond formation on electrode surfaces, producing C_{2+} products with decent selectivity as well as good efficiency has proven to be considerably difficult [34]. Among all kinds of state-of-the-art catalysts, Cu-based catalysts seem to be the most efficient and promising material for the CO_2RR toward multicarbon products [35]. Specifically, numerous studies have focused on the direct CO_2RR toward acetate using Cu as a key component. Briefly, we summarize the representative CO_2RR catalysts for acetate production in Figure 1. For example, Meyer and coworkers reported high CO_2-to-acetate efficiency (21.2% Faradaic efficiency (FE) at −1.33 V in 0.5M $KHCO_3$) by using the electrochemically reduced monodispersed mixtures of Cu and Ag nanoparticles on electrochemically polymerized poly-Fe(vbpy)$_3$(PF$_6$)$_2$ films [36]. A possible initiator for C—C bond formation in acetate production may be the capture of *CH_2 on Cu sites and its further combination with CO produced by neighboring Ag. Similarly, Basile and coworkers synthesized a Cu_2O—Cu^0 catalyst by the electrodeposition of Cu metal on a carbonaceous membrane, which achieved a high selectivity (76% FE) toward acetic acid [34]. Moreover, compared with traditional copper-based catalysts, isolated copper centers show favorable selectivity in the direct CO_2RR toward acetate. For example, a conductive covalent organic framework with isolated copper sites was designed by Liao and coworkers, it was proven to be an excellent electrocatalyst for the reduction of CO_2 to acetate with an FE of 90.3% at a current density of 12.5 mA cm^{-2} in 0.1 M $KHCO_3$ solution [37]. Apart from copper-based electrocatalysts, there has also been a notable development in nonmetallic and other metal-based electrocatalysts for the direct conversion of CO_2 to acetic acid/acetate. For instance, nitrogen-doped nanodiamond on a silicon rod array was developed by Liu et al. for selective acetate production from CO_2RR [33].

Figure 1

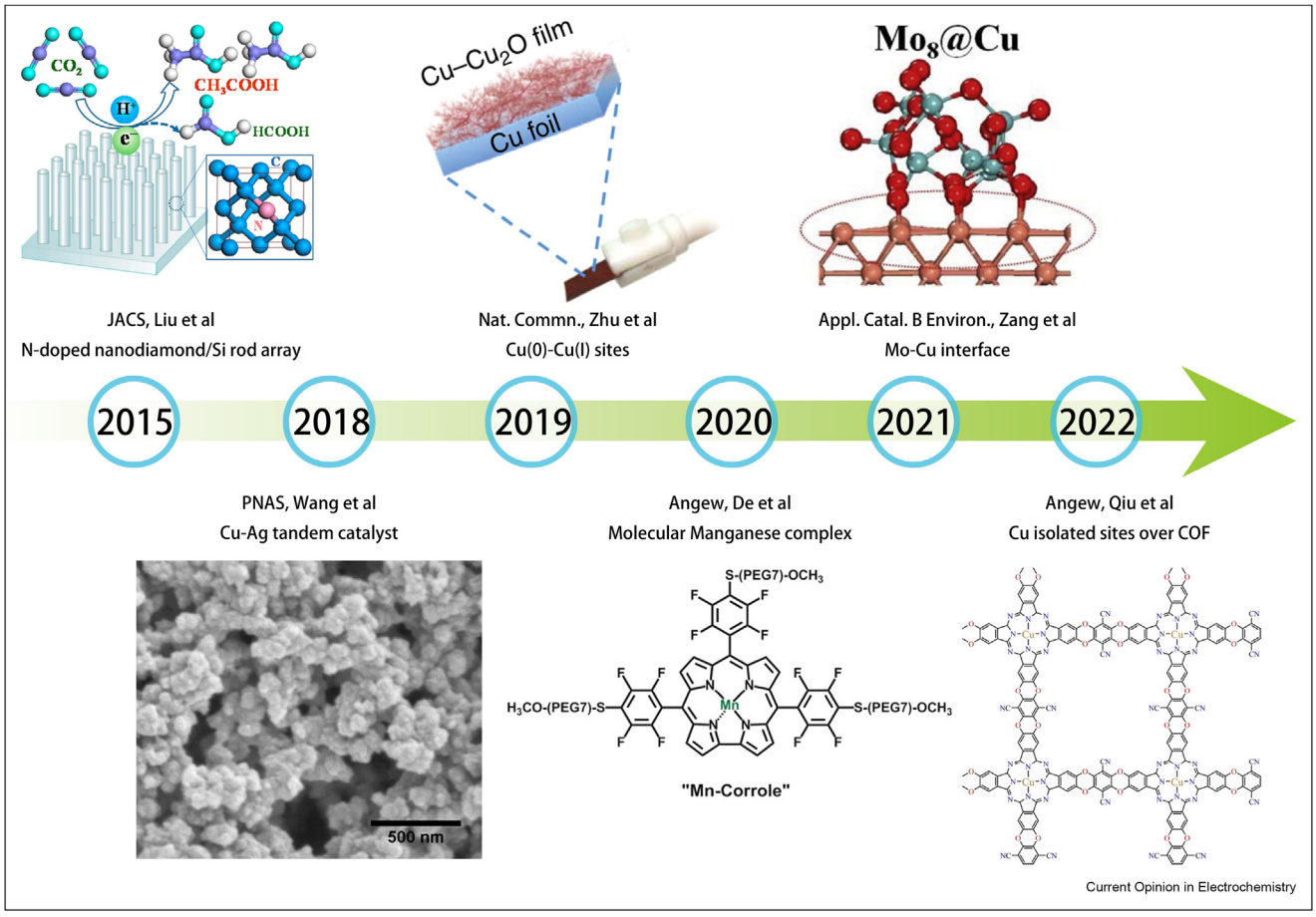

A brief history of the representative progress of CO_2RR to acetic acid. To date, various sophisticated catalysts have been claimed to be effective for CO_2-to-acetate process. 2015, NDD/Si RA was initially investigated for CO_2RR to acetate. This figure is reproduced from the study by Liu et al. [33] with the permission from the American Chemical Society, copyright 2015. 2018, the concept of tandem catalyst was applied to circumvent the obstacle in direct CO_2RR. This figure is reproduced from Wang et al. [36] with the permission from the Proc. Natl. Acad. Sci. U. S. A., copyright 2018. In 2019, Cu(0)-Cu(I) site was firstly investigated for acetate production. This figure is reproduced from the study by Zhu et al. [40] with the permission from Spring-Nature, copyright 2019. 2020, Mn-based molecular catalyst was proposed for effective acetate generation from CO_2. This figure is reproduced from the study by De et al. [38] with the permission from the Wiley-VCH, copyright 2020. 2021, Zang et al. proposed Mo–O–Cu interface promote acetate formation. This figure is reproduced from the study by Zang et al. [45] with the permission from the Elsevier, copyright 2021. 2022, Qiu et al. further designed a COF structure to modulate electronic structure of isolated Cu to enhance acetate selectivity. This figure is reproduced from the study by Qiu et al. [37] with the permission from the Wiley-VCH, copyright 2022.

In addition, well-designed molecular metal complexes containing manganese or cobalt were also developed to directly reduce CO_2 toward acetic acid/acetate. In one study by Schçfberger and cooperators, a molecular Mn^{III}-corrole complex was designed for the direct and selective production of acetic acid from CO_2 with a FE of 63% [38]. In another study, they observed that the Co(III) triphenylphosphine corrole complex exhibited potential-dependent CO_2 reduction to produce low amounts of acetic acid with an FE of 13% [39].

Summary of several typical mechanisms

Although the formation of acetate in the CO_2RR has been intensively studied via well-developed characterization techniques, there is still no conclusive answer to the exact reaction pathway and mechanism of such conversion. Indeed, the mechanism of C–C formation during the CO_2RR toward acetate/acetic acid is still debatable [36]. According to recent research, it has been widely accepted that *COOH is a rate-determining intermediate, it may follow several typical proposed pathways toward the formation of acetate (as summarized in Figure 2): (1) the generation of *CO and subsequent dimerization of another *CO intermediate, (2) the generation of $*CH_3$ and successive coupling with CO_2 insertion, (3) the formation and further reduction of an oxalate intermediate, and (4) the disproportionation of acetaldehyde, which is promoted by the local alkaline environment in the vicinity of the electrode surface.

Figure 2

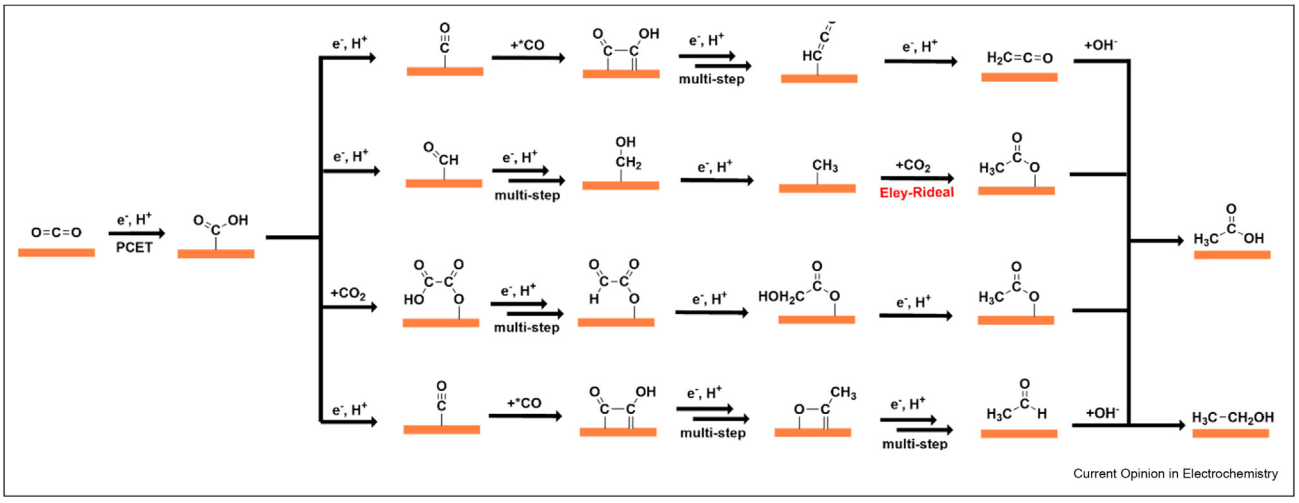

Typical mechanisms for direct CO_2RR toward acetate/acetic acid.

*Via dimerization of the *CO intermediate*

Among all the proposed mechanisms, the *CO dimerization pathway tends to receive the most attention: CO_2 is initially reduced to absorbed CO which generate hydrocarbons and oxygenates by dimerization on metallic catalysts such as copper [41,42]. Numerous studies have been developed to demonstrate this process in recent years. For instance, Han and coworkers reported the CO_2RR to acetic acid over a three-dimension dendritic Cu—Cu_2O composite, which achieved an over potential of 0.53 V versus reversible hydrogen electrode (*vs.* RHE) and an FE of 48% in KCl aqueous solution [40]. Some control experiments and infrared-spectra studies were conducted to explore the presence of possible intermediates, such as CO and acetaldehyde. The results showed that the *OCCHO intermediate, which could be further reduced to CH_3COO^- species at the electrode surface, was critical for the formation of acetic acid. In another study, a stable π-π stacking framework formed by the trinuclear copper compound $Cu_3(HBtz)_3(Btz)Cl_2$ with pyrazolate-bridged dicopper sites was developed by Zhu et al. for CO_2RR. *In situ* infrared spectroscopy, density functional theory calculations, and control experiments revealed that the formation of *OCCHO intermediate from *CO dimerization was the key step for yielding C_{2+} products [43]. The synergistic effect between the highly active dicopper site and the nearby proton relay promoted C—C coupling by reducing the Gibbs free-energy barrier for *CO hydrogenation. As a result, an enhanced CO_2RR efficiency toward C_{2+} products was observed. Similarly, in a study of a Cu—CuI composite catalyst with abundant Cu^0/Cu^+ interfaces, Wang and coworkers revealed that the adsorbed iodine species promote C—C coupling by influencing the adsorption of the *CO intermediate [44]. As such, it can be deduced that *CO may be the key intermediate for *OCCHO formation during the acetate/acetic acid production process.

*Via *CH_3 intermediate coupling with CO_2 insertion*

While the former mechanism acquires coupling between *CO intermediates and keeps the C—O bond intact, some researchers have pointed out that the reaction pathway above must continuously overcome a high energy barrier in *OCCHO formation [27]. There will be immense restrictions on the formation of acetate/acetic acid during the CO_2RR. Therefore, a new pathway is proposed, which assumes *CH_3 was initially produced by several hydrogenation steps and then acetate formation takes place via the coupling of CO_2 molecules with nearby *CH_3. The produced *OOC_2H_3 can subsequently undergo a simple protonation step and desorbed from the catalyst surface. Taking Mo_8O_x/Cu heterostructures as an example, Wei and coworkers reported a high FE of 49% toward acetate at 110 mA cm^{-2} with a relatively low applied potential of −1.13 V *vs.* RHE [45]. Based on density functional theory (DFT) calculations as well as experimental results, the designed Cu—O—Mo interface catalyst was demonstrated to promote the generation of *CH_3 and its successive coupling with CO_2 under an applied potential. Experimental observations conducted by Genovese et al. also proved the reliability of acetate formation via the coupling of the *CH_3 intermediate with the CO_2 insertion [46]. Using copper nanoparticles on carbon nanotubes, they observed no generation of *CO during the first step in the CO_2RR, which was a prerequisite to forming C—C bonds through the *CO dimerization pathway. In contrast, theoretical calculations and *in situ* infrared spectroscopy revealed that the combination of *CO_2^- with the reduced species *CH_3 on the catalytic surface led to acetate formation. Considering that the

absorbed $*CH_3$ species can easily undergo a nucleophilic attack from the radical anion $*CO_2^-$, such a reaction is quite favorable. In addition, a recent study revealed the same pathway using a covalent organic framework with an isolated copper-phthalocyanine active site for the CO_2RR toward acetate [37]. With the help of theoretical calculations and *in situ* infrared spectroscopy, it was concluded that the isolated copper-phthalocyanine active site with high electron density was conducive to the coupling of $*CH_3$ with CO_2 to produce acetate while preventing the coupling of *CO with *CO or *CHO to produce ethylene and ethanol.

Via an oxalate intermediate

It was first reported by Jaramillo et al. that enol-like intermediates might be involved in CO_2RR toward a wide range of C_{2+} products on metallic copper surfaces [47]. In their study, the researchers used copper as the catalyst across a range of potentials for CO_2RR and observed a total of 16 different CO_2 reduction products, 11 of which are C_{2+} oxygenates. Then, they concluded that enol-like surface intermediates might account for the observed selectivity for these distinct C_{2+} oxygenates: including aldehydes, ketones, alcohols, and carboxylic acids. Later, based on the *in situ* infrared spectrum results, along with the above-proposed reaction mechanisms, Quan and coworkers demonstrated a possible CO_2-to-acetate pathway via an oxalate intermediate on an N-doped nanodiamond/Si rod array (NDD/Si RA) electrode [33]. According to their results, the peak at 1307 cm^{-1} in the infrared spectrum was attributed to $*OOC\text{-}COO^-$. The peak intensity initially increased but later remained unchanged during further electrolysis, suggesting that $*OOC\text{-}COO^-$ might be the intermediate of CO_2 RR. As such, the possible reaction pathway associated with an oxalate intermediate was proposed: CO_2 was first adsorbed on the electrode surface and reduced to $*CO_2^-$, after which the formed $*CO_2^-$ radical combined with another CO_2 and generated $*OOC\text{-}COO^-$. The oxalate intermediate was then protonated and further reduced, resulting in the production of acetate. In addition, Sun et al. proposed a similar pathway of $CO_2 \rightarrow *COOH^- \rightarrow *OOC\text{-}COO^- \rightarrow CH_3COO^-$ based on an *in situ* diffuse reflectance Fourier transform infrared spectroscopy study, while ultrathin $WO_3 \cdot 0.33H_2O$ nanotubes was investigated as the model catalyst [48]. It was claimed that if *H radicals around early formed *COOH intermediates were insufficient, adjacent *COOH radicals tended to form C–C bonds and generate HCOO–COOH intermediate. Subsequently, the hydrogen bond connected –COOH undergoes proton-coupled electron transfer (PCET) until it was reduced to $-CH_3$, after which the acetum product would be formed. In addition to experimental proofs, DFT calculations conducted by Schçfberger and cooperators. Also substantiated this mechanism [38]. Taking the model of a molecular Mn^{III}-corrole complex on the three meso-positions with polyethylene glycol moieties, as an instance, they showed that C–C dimerization would lead to the oxalate-type intermediate formation and its consecutive reduction resulted in the formation of acetate. Moreover, further electroreduction experiments of oxalic acid toward acetic acid also strongly supported this mechanistic pathway and proved its credibility.

Via disproportionation of acetaldehyde

Unlike the aforementioned mechanisms, the pathway via acetaldehyde disproportionation is also proposed based on a series of interesting experimental results. For instance, Kanan's group noticed that during CO reduction at high pH, acetate formation would be enhanced, accompanied by a notable decrease in ethanol concentration on oxide-derived Cu, which suggested a correlation between these two C_2 species [49]. In other words, ethanol and acetate are likely to be mechanistically linked and thus share the same selectivity-determining intermediates and/or steps. In addition, when searching for evidence for product-specific active sites on oxide-derived Cu catalysts for CO_2RR, Lum and coworkers also found that ethanol and acetate shared the same active site for the C–C coupling [35]. However, they did not point out the exact intermediate species. Actually, some previous studies have already reported that ethanol and acetate were the disproportionation products of acetaldehyde, although not under electrocatalytic conditions. For example, as early as 1980 [50], Maitlis and coworkers reported a homogeneous disproportionation of acetaldehyde into ethanol as well as acetic acid by the catalyzation of rhodium hydride complexes. Later, Nagai et al. demonstrated that acetaldehydes underwent a noncatalytic self-disproportionation reaction producing ethanol and acetic acid in supercritical water at 400 °C [51]. As such, it can be inferred that ethanol and acetate may share a common intermediate during direct CO_2RR toward acetic acid/acetate. It was not until Koper and cooperators used a seemingly catalytically inactive electrode, boron-doped diamond, to conduct CO_2RR at very cathodic potentials that the pathway from acetaldehyde disproportionation was clearly proven [52]. They pointed out that the disproportionation of aldehydes, which could be promoted by the local alkaline environment in the vicinity of the electrode surface, accounted for the formation of carboxylic acids and alcohols. Additionally, this phenomenon can also be observed in other aldehydes in their experiments, which probably explains the concomitant formation of acids and alcohols during the CO_2RR [40].

Catalyst design for direct conversion

As mentioned above, with the aid of quantum chemical calculations and operando spectroscopy, several possible pathways of acetic acid/acetate formation have been heavily studied. To improve the selectivity and productivity of the direct CO_2RR toward acetic acid/acetate,

the concentration of intermediate species plays a negligible role. Only sufficient amounts of intermediate species are generated in the surroundings of active sites will C_2 products such as acetic acid be generated during CO_2RR. In this section, we highlight the electrocatalyst design strategies focusing on improving the concentration of different intermediate species. For clarity, the representative reported catalysts in literature about CO_2-to-acetate process are listed in Table 1.

The most common way to improve the CO_2RR performance toward acetate/acetic acid is to manipulate the local electronic structures of the electrocatalysts, by which their oxidation states can be tuned. Since copper-based electrocatalysts have shown exceptional performance in C—C coupling during the direct CO_2RR to C_{2+} products, using different nonmetallic atoms or dopants to regulate the oxidation states of Cu seems to be a promising strategy. One example is the Cu—Cu_2O/Cu electrode prepared by Han and coworkers, which showed outstanding catalytic performance for CO_2 reduction to acetate in a KCl aqueous electrolyte [40]. At −0.4 V *vs.* RHE, the overpotential for acetic acid was 0.53 V when the FE of C_{2+} products reached 80.7% at a current density of 11.5 mA cm^{-2} (Figure 3a and b). The authors attributed this extraordinary electrocatalytic activity to the synergistic effects of the optimal Cu (I)/Cu (0) ratio. As proposed by Xiao et al., the adsorbed CO on Cu (I) sites is positively charged while CO on Cu (0) is negatively charged, accounting for lower dimerization Gibbs energy barriers among adjacent Cu (I)—Cu (0) sites [53]. In addition to oxygen, heteroatoms such as halides and nitrogen have also been intensively investigated to tune the Cu oxidation state for promoting C—C coupling during CO_2RR. Li et al. designed a Cu—CuI composite catalyst with abundant $Cu(0)/Cu^+$ interfaces by physically mixing Cu nanoparticles and CuI powders, which achieved a remarkable C_{2+} partial current density of 591 mA cm^{-2} at −1.0 V *vs.* RHE in a flow cell (Figure 3c) [44]. It was believed that the Cu^+ species stabilized by the adsorbed iodine species, together with adjacent metallic Cu sites, were the active sites to promote C—C coupling.

Designing tandem catalysts is another promising strategy to enhance C—C coupling. It is commonly accepted that adsorbed *CO species act as key intermediates for C_{2+} compounds, and Cu-based catalysts generally lack adequate CO coverage in the CO_2RR, leading to undesirable C_{2+} selectivity. As a solution, tandem electrocatalysts have been proposed in recent years [28,36,55—57]. The general idea of tandem catalysts is that two active sites coexist adjacently and undertake different tasks. One site, such as Ag and Zn, serves as a CO formation site, while the CO conversion site reduces CO toward C_{2+} products. Under this principle, bimetallic [28], core—shell [57] and dual-single atom catalysts [58] are proper alternatives to design tandem catalysts. Taking the ultrasmall $(Cu)_n$, $(Ag)_m$ bimetallic nanoparticles as an example, it was reported that the electrochemically reduced Cu and Ag clusters could achieve an FE of 21.2% for acetate at −1.3 V *vs.* RHE in 0.5 M $KHCO_3$ [36], as shown in Figure 3d. The Ag-catalyzed formation of CO followed by its capture on neighboring Cu sites is the proposed mechanism for C—C bond formation. Additionally, Ager and coworkers developed a bimetallic pattern compromising interdigitated and independent Au and Cu sites (26 μm spacing apart) over SiO_2 for the CO_2RR, as shown in Figure 3e [54]. In the calculated model, the Au site generated a locally concentrated CO environment, while Cu served to provide the active sites for C—C coupling by utilizing the spread CO molecules (Figure 3f). To enhance CO utilization while suppressing hydrogen production, they also directly deposited Cu sites onto Ag substrate. Consequently, controlling the relative areas of the two metal patterns would tune the ratio of oxygenate to ethylene from 0.59 (Ag was 100% covered by Cu) to 2.39 (Ag was 2.4% covered by Cu). As above, the combination of two different metals together plays an important role in the deep conversion of CO_2 to acetate/acetic acid.

Table 1

Performance of catalysts investigated for CO_2RR toward acetate.

Catalyst	$FE_{acetate}$ (%)	Current density (mA cm^{-2})	Potential (V vs. RHE)	Stability (h)	Reactor	Electrolyte	Reference
$(Cu)_n(Ag)_m$	21.2	–	−1.33	–	H Cell	0.5M $KHCO_3$	[36]
Cu_2O–Cu^0	76	0.46	−0.4	5	H Cell	0.3M $KHCO_3$	[34]
Cu–Cu_2O-2	48	11.5	−0.4	24	H Cell	0.1M KCl	[40]
PcCu-TFPN	90.3	12.5	−0.8	–	Flow Cell	0.1M $KHCO_3$	[37]
Mn-corrole	63	–	−0.674	5	H Cell	0.1M phosphate buffer (pH 6)	[38]
Co-corrole	13	2.9	−0.955	5	H Cell	0.1M $NaClO_4$ with phosphate buffer	[39]
NDD/Si RA	77.3	~1	−0.8	–	H Cell	0.5M $NaHCO_3$	[33]
$Cu_3(HBtz)_3(Btz)Cl_2$	4.7	7.9	−1.3	24	H Cell	0.1M $KHCO_3$	[43]
Cu–CuI	<5	894	−1.0	85	Flow cell	1M KOH	[44]
Mo_8O_x/Cu	48.68	~110	−1.13	–	Flow cell	saturated $NaHCO_3$	[45]

Figure 3

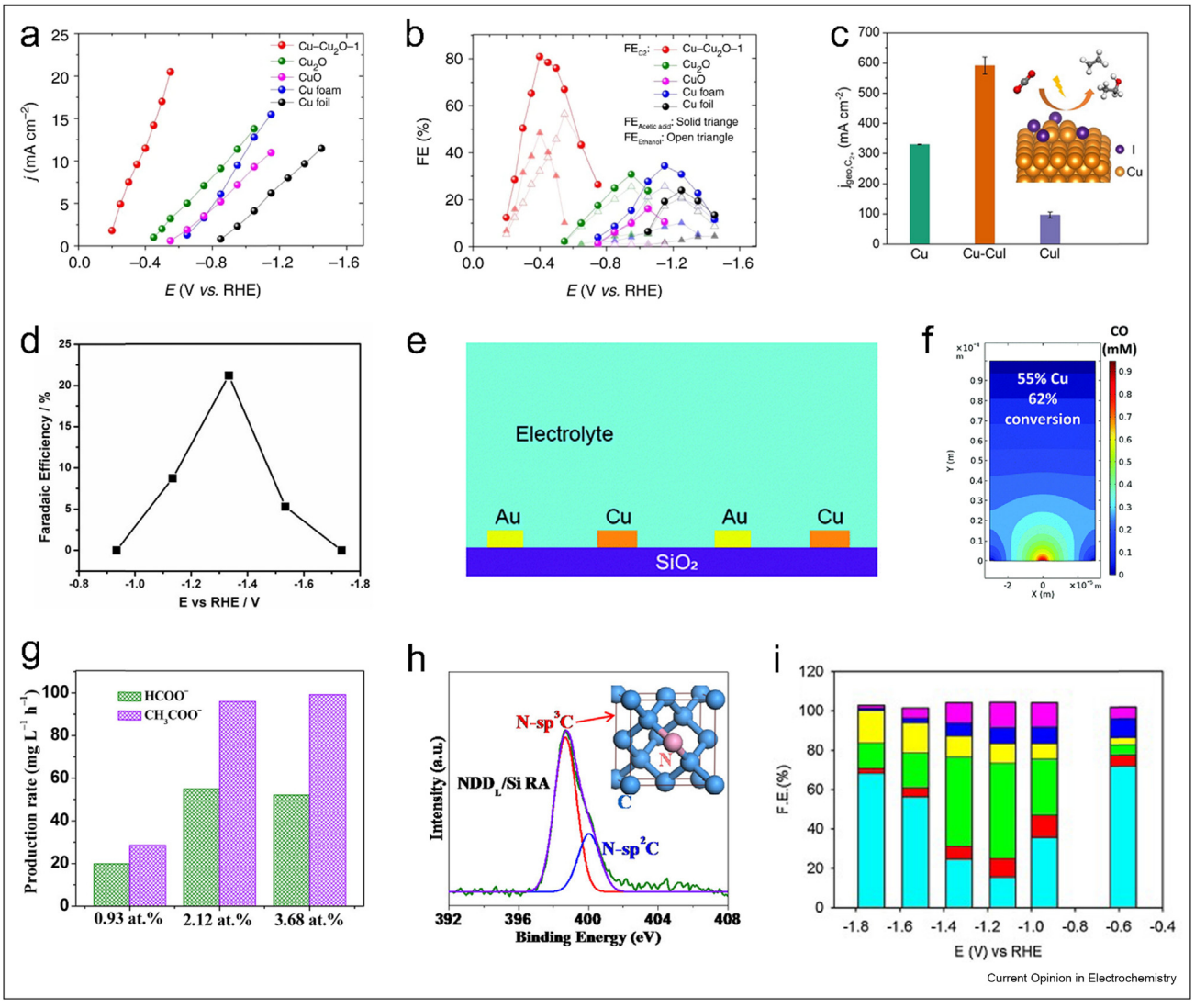

(**a**) Total current density at various potentials over copper-cuprous oxides and normal Cu-based catalysts. (**b**) C_{2+} oxygenates (ethanol and acetate) selectivity for the CO_2RR at different applied potentials (vs. RHE). (**a**) and (**b**) are reproduced from the study by Zhu et al. [40] with the permission from Spring-Nature, copyright 2019. (**c**) C_{2+} partial current density and catalytic scheme of the Cu−CuI composite catalyst compared with Cu or CuI alone. (**c**) Is reproduced from the study by Li et al. [44] with the permission from Wiley-VCH, copyright 2021. (**d**) Faradaic efficiency for Cu_2Ag_3 at different applied potentials in CO_2-saturated 0.5 M $KHCO_3$. (**d**) Is reproduced from the Wang et al. [36] with the permission from Proc. Natl. Acad. Sci. U. S. A., copyright 2018. (**e**) Scheme of interdigitated Cu and Au bimetallic electrodes. (**f**) Calculated CO concentration contours in mM for interdigitated devices with relative area coverages of 55% Cu. (**e**) and (**f**) are reproduced from the study by Lum et al. [54] with the permission from the Royal Society of Chemistry, copyright 2018. (**g**) The relation between N content and production rate of acetate and formate over NDD/Si RA. (**h**) N 1s XPS spectrum of NDD_L/Si RA, indicating N dopant configuration. (**g**) and (**h**) are reproduced from the study by Liu et al. [33] with the permission from the American Chemical Society, copyright 2015. (**i**) Faradaic efficiencies of each CO_2RR peak with potential dependence over Mo_8O_x/Cu catalyst (cyan: hydrogen, red: ethanol, green: acetate, yellow: methane, blue: ethylene, purple: ethane). (**i**) Is reproduced from the study by Zang et al. [45] with the permission from the Elsevier, copyright 2021.

In addition to the abovementioned catalyst design strategies, well-designed molecular metal complexes have recently been developed to reduce CO_2 to multi-carbon products. In a study of a cobalt(III) triphenyl-phosphine corrole complex, Roy and coworkers revealed that the corrole molecule tends to stabilize different radical intermediates, such as COOH• and HCO•, at the metal site [39]. Since the intermediate species could be well stabilized at the active sites, highly reduced products would be formed when sufficient amounts of electrons are provided. Under a moderately acidic aqueous medium (pH 6), the main reduction products were formic acid, methanol, and acetic acid. Later, they designed a molecular Mn^{III}-corrole complex to directly and selectively produce acetic acid from CO_2 [38]. Further studies reveals that electroactive Mn^{II}

species play a similar role, which bind with CO_2 and stabilizes the reduced intermediates during CO_2RR. The Lewis acidity of the Mn^{III} center had a higher tendency to bind with the Lewis basic O-site of the carboxyl group, which would facilitate C—C coupling to form an oxalate-type intermediate. As a result, the catalyst shows a superior acetic acid selectivity of over 40% in constant electrolysis in phosphate buffer.

Finally, creating electrocatalyst defects by heteroatoms or cluster doping represents another alternative strategy to modulate catalytic selectivity as well as activity. For example, Quan et al. incorporated N atoms into nanodiamond rod arrays and achieved a >75% FE for the acetate [33]. As shown in Figure 3g, heavier N doping in NDD/Si RA remarkably promotes the CO_2RR reaction rates. X-ray photoelectron spectroscopy (XPS) results validated that dominate N species is doped in carbon lattice with sp^3 configuration (Figure 3h), which undergo a special CO_2RR path through oxalate intermediates to generate acetate in in-situ infrared spectra. The modification of small clusters may also lead to superior activity. Bao and cooperators reported an interface engineering strategy to modify copper nanocubes with polyoxometalate to generate a Mo_8O_x/Cu interface as active sites for the CO_2RR toward acetate [45]. DFT calculations suggested that the interface of Cu planes and Mo_8O_x cluster promoted the generation of $*CH_3$ and its successive coupling with CO_2, which resulted in an acetate FE of 48.7% under a current density of 110 mA cm^{-2} at −1.13 V *vs.* RHE (Figure 3i). Notably, such a metal-oxygen-metal interface design not only exhibits a remarkable electron reservoir but enables the synergetic effect between Mo_8 and Cu. As such, this can be a general model for the rational design of catalysts in CO_2RR toward acetate/acetic acid.

Overall, various catalysts have suggested effective acetate selectivity improvement. As displayed in previous sections, constructing Cu(0)-Cu(I) sites would boost C_{2+} products, but it is hard to suppress competitive byproducts (ethylene and ethanol). A tandem catalyst ingeniously harmonizes the CO_2-to-CO process and CO-to-acetate process in a sole catalyst. Regarding *CO is actually the key intermediate in acetate generation, more efforts must be invested to promote tandem catalyst application. Molecular metal complexes are a class of catalysts recently developed for CO_2RR. Although ambiguity may exist in the relationship between activity and coordination effects, adjusting ligand's structures can exquisitely regulate electronic structures, offering more opportunities to generate rare products. Based on the structure—property relationship, the unprecedented FE is achieved in NDD/Si RA catalyst aforementioned, proving the elaborate doping strategies is suitable for unitary selectivity. However, the development of CO_2-to acetate is quite sluggish. Firstly, none of the reported catalysts can directly electro-convert CO_2 into acetate with an industrial-scale partial current (>200 mA cm^{-2}). Secondly, most of the reported catalysts are sophisticated for synthesis hampering commercial application. Resorting to a convenient synthetic process should be predominant in the near future. Finally, we still have to suppress ethanol and formic acid formation simultaneously to lower separation cost, as those co-products are in liquid phase. Given the high threshold in scalability, indirect routes to convert CO_2 into acetate will be discussed in the next section.

Indirect CO_2RR toward acetate

The driving force behind indirect CO_2RR

Direct CO_2 conversion toward acetate is potentially more energy efficient, but the drawbacks of CO_2 electrolysis are not negligible. To improve the selectivity while suppressing the hydrogen evolution reaction (HER) during the CO_2RR, CO_2 electrolysis is always applied in an alkaline media [59]. However, the formation of carbonate not only results in (bi)carbonate precipitation in the gas diffusion electrode (GDE) thus damaging the operation stability [60], but also imposes extra energy loss due to CO_2 regeneration [61]. The CO_2RR in acidic media offers an avenue to avoid carbon loss, but the products are inevitably dominated by HER and C_1 products [62]. Moreover, the liquid products of the CO_2RR are in great varieties, including formic acid, ethanol, acetic acid, acetaldehyde and propanol, leading to a daunting task for separation [63]. In this case, indirect CO_2RR integrating the CORR process provides us with an alternative solution to address these issues. The CO_2RR and CORR to the acetate process are presented by the equation below [64]:

$$2CO_2+8H^++8e^- \rightarrow CH_3COOH+2H_2O \qquad E_0 = 0.12\,V\ (vs.\ RHE)$$

$$2CO+4H^++4e^- \rightarrow CH_3COOH \qquad E_0 = 0.32\,V\ (vs.\ RHE)$$

CORR toward acetate has a higher thermodynamic potential than CO_2RR toward acetate (0.32 V *vs.* 0.12 V), and it involves fewer proton-coupled-proton transfer steps. These inherent properties indicate that the CO-to-acetate process may have a higher activity than the CO_2-to-acetate process [64]. In addition, CO is inert in the reaction with hydroxide ions, resulting in no carbon loss [65]. Kanan and coworkers designed a special cell architecture that achieved 68% CO single-pass conversion and 75% FE for acetate production [65]. Although the solubility of CO is relatively low (1 mM), a high partial current (>100 mA cm^{-2}) was achieved in this work owing to the special GDE design and unprecedented high pressure (4 bar) of CO feedstock. Consequently, one can turn to split the CO_2-to-acetate process into two consecutive procedures, CO_2-to-CO and CO-to-acetate, as an alternative solution for the CO_2-to-acetate process.

Recent development of CO_2RR to CO

Compared with the immature direct CO_2-to-acetate process, the techniques for CO_2-to-CO have been widely available with high selectivity and efficiency. Wang's group designed a large-scale CO_2RR catalyst based on single Ni atoms on the commercial carbon black [8]. In a 10*10 cm^{-2} membrane electrode assembly (MEA) reactor, it reached nearly 100% selectivity and a 3.42 L per hour CO generation rate under 8.3 A current. Similarly, another recent work also achieved near 100% CO FE at a current density of 1.2 A cm^{-2} over 360 h of continuous operation among metalloporphyrin-linked mercurated graphynes [66]. Very recently, a polytetrafluoroethylene (PTFE) nanoparticle-modified Ni—N—C catalyst was synthesized for the CO_2-to-CO process in the acid media [67]. In this work, the CO_2 single-pass utilization reached 75.7% at 200 mA cm^{-2}, and it steadily operated in pH 2 media for more than 36 h without any selectivity (100% for CO) decay. As above, these viable schemes ensure the feasibility of efficient CO production from CO_2. To meet the industrial demand for scaling up the traditional CO_2RR, Endrődi et al. constructed a multilayer CO_2 electrolyzer stacks and arranged multiple electrolyzer layers into an intact zero gap cell that could be operated under a pressurized gas feed without a liquid catholyte [68]. This novel design offered numerous advantages: it markedly decreased the total cell resistance and carbon loss, as well as simultaneously achieving high CO_2 conversion (40%), CO FE (95%), and current density (above 250 mA cm^{-2}) under a fast CO_2 feed rate (above 500 sccm). Moreover, this innovative design is more compact and integrated than a traditional electrolyzer, which is conducive to subsequent improvement. For short, we list some recent literature about CO_2RR to CO for curious readers [69—75].

Development of CORR toward acetic acid/acetate

Unlike the direct conversion of CO_2 to acetic acid (acetate), CORR offers a novel route with high selectivity and efficiency [64]. Recent studies have been devoted to creating efficient catalysts and electrolyzers for acetate formation in the CORR, together with elucidating the mechanisms. As displayed in Figure 4, a brief history of representative CORR to acetate production is presented. In 2014, Kanan's group observed that acetate selectivity increased with pH among oxide-derived Cu (OD-Cu) [49]. Later, Jouny et al. circumvented the intrinsic low CO solubility problem by incorporating gas-diffusion electrodes in the CO-to-acetate process [76]. Since then, a series of well-designed catalysts and CO electrolyzers have been profoundly studied to produce high-concentration acetate solutions. In 2019, Kanan and cooperators constructed interdigitated flow fields to maximize the flux of CO and continuously produced concentrated acetate [65]. To reduce the separation cost, a porous solid electrolyte (PSE) was further incorporated to replace traditional liquid media, which generated a 0.33 M acetic acid solution without any impure ions [77]. In 2022, Ji et al. reported a CuPd intermetallic compound that exhibited 70% acetate FE under a 500 mA cm^{-2} current density and the catalyst steadily operated up to 500 h [78]. Very recently, Jiao et al. fully utilized the ethanol permeability of an anion-exchange membrane (AEM) to generate ultra-pure acetate solution with a concentration as high as 7.6 M [79].

Despite the vigorous development of CO-to-acetate, further progress is still required for large-scale production. Martin et al. thoroughly calculated the required parameters to commercialize CO_2RR [80], which is also suitable for CORR process [64]. To make the whole process economic, the threshold current density is beyond 200 mA cm^{-2}, and the FE for C_{2+} products should be over 80%. As for stability, the whole electrolyzer should constantly operate for more than 5000 h with an overpotential lower than 0.4 V for practical application. Besides, the full cell energy conversion efficiency should surmount 60% [81]. The most important part to approach scalability is to design efficient catalysts, but the selectivity and activity of the CORR are structure-sensitive, making it difficult to design desirable catalysts. In the following discussion, we present guidelines for designing highly active catalysts based on insights into previously reported reaction mechanisms. The ultimate goal is to establish a general design principle for developing catalysts and reactor systems with high activity, selectivity, stability, and scalability.

Several plausible mechanisms

The mechanism of the CO-to-acetate process has been profoundly studied by researchers with the assistance of DFT calculations and kinetic experiments. Based on the isotope-labeled and in-situ mass spectra, three possible mechanisms are widely accepted for acetate generation. Generally, the most accepted mechanism was proposed by Kanan et al. [49] and further validated by subsequent experimental evidence [77,78,82—84]. In this route (Figure 5a, Route 1), acetate is generated via surface-bound ethenone, which favors nucleophilic attacks from solvent. In this process, the formation of *OCCOH species is identified as the rate-determining step to produce *CCO, which acts as the precursor of ethenone. In detail, the adsorbed *CO species is dimerized to *OC-CO followed by PCET to generate *OC-COH, which is known as the common intermediate to ethylene, ethanol, acetate and other oxygenates. *In situ* Fourier transform infrared spectroscopy has demonstrated solid evidence that *OC-COH species associated signals at 1584 and 1191 cm^{-1} were successfully observed during CO_2RR [85—88]. The following steps diverge into two routes: *OC-COH further generates *HOC—COH by PCET or forms *CCO when *OH breaks away from *OC-COH [77]. Koper et al. suggested that *CCO might transform to *HC-CO and *HC-CHO through PECT to generate ethanol [85].

Figure 4

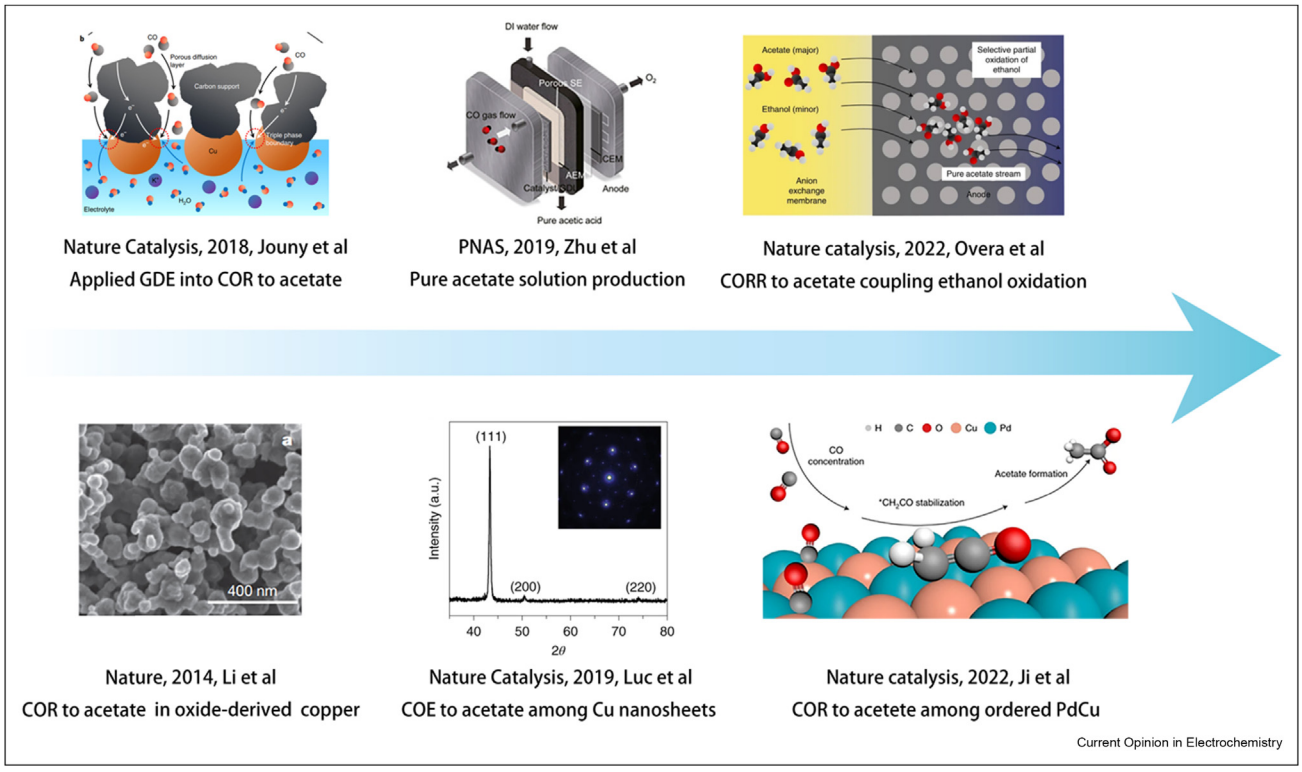

A brief history of the representative progress of CORR to acetic acid. Until 2022, novel electrolyzer and catalyst design have been vigorously developed, and the FE, current density and total energy efficiency have been remarkedly improved. 2014, OD-Cu was initially investigated for CORR to C_{2+}. 2018, GDE was applied in CORR electrolyzer to achieve high current density. 2019, Cu exposed (111) facets was proved to be effective for acetate production. These three figures are reproduced from the studies by Li et al., Jouny et al., Luc et al. [49,76,82] with the permission from the Spring-Nature, copyright 2014, 2018, 2019. The same year, the porous solid electrolyte was used to produce pure acetic acid solution. This figure is reproduced from the study by Zhu et al. [77] with the permission from Proc. Natl. Acad. Sci. U. S. A., copyright 2019. 2022, CuPd intermetallic compound was proved to be highly effective for acetate production. The same year, Jiao's group proposed a novel strategy to convert ethanol by-product into acetate, which may decrease separation cost. These two figures are reproduced from the studies by Ji et al., Overa et al. [78,79] with the permission from the Spring-Nature, copyright 2022.

However, Luc et al. figured out that *CCO could also transform into $*H_2C{=}CO$ [82]. Importantly, $*H_2C{=}CO$ is commonly recognized as surface-bound ethenone, which forms acetate through hydration (Figure 5a).

To verify this mechanism, isotopic labeling together with a gas chromatography-mass spectrometry (GC–MS) system was used to analyze the liquid products. As shown in Figure 5b, isotopically labeled $C^{18}O$ was fed to probe key intermediates on OD-Cu. To ensure accuracy, no oxygen exchange would happen between the feedstock and solvent, circumventing the interference signals [76]. From fragment patterns, the introduction of $C^{18}O$ led to partially labeled acetic acid at 62 amu, i.e., $CH_3C^{18}O^{16}OH$. Since ^{16}O only originates from the solvent, it can be concluded that one H_2O or hydroxide ion participated in the reaction with a certain intermediate. Moreover, a slight signal presents at 64 amu, i.e., $^{12}CH_3^{12}C^{18}O^{18}OH$ or $^{13}CH_3^{13}C^{18}O^{16}OH$ is observed compared with 62 amu when using $C^{16}O$ (corresponding to $^{13}CH_3^{13}C^{16}O^{16}OH$). The 64 amu signal when using $C^{18}O$ might arise from $^{12}CH_3^{12}C^{18}O^{18}OH$ species (the double-labeled product) rather than the interference of natural ^{13}C. These results are consistent with the $H_2^{18}O$ experiments by Lum et al. [90]. To summarize the experiments, the predominant mechanism certainly contains an intermediate with only one oxygen, and it subsequently undergoes an addition reaction by a solvent oxygen atom. Meanwhile, a small fraction of acetate is double-labeled in the presence of $C^{18}O$, which indicates that some other mechanism may also exist and will be discussed further. On the other hand, ethanol was partially labeled, and acetaldehyde was unlabeled. Because only acetaldehyde can exchange oxygen atoms with solvent [91], the partially labeled ethanol might be generated via a distinct acetaldehyde-related route. Toward a direct verification of the ethenone mechanism, Jiao et al. introduced NH_3 to co-feed the CORR over a Cu catalyst [83]. Owing to the high nucleophilic ability of NH_3, the highly active ethenone structure was easily attacked by nitrogen atoms, resulting in C–N coupling. Figure 5c

Figure 5

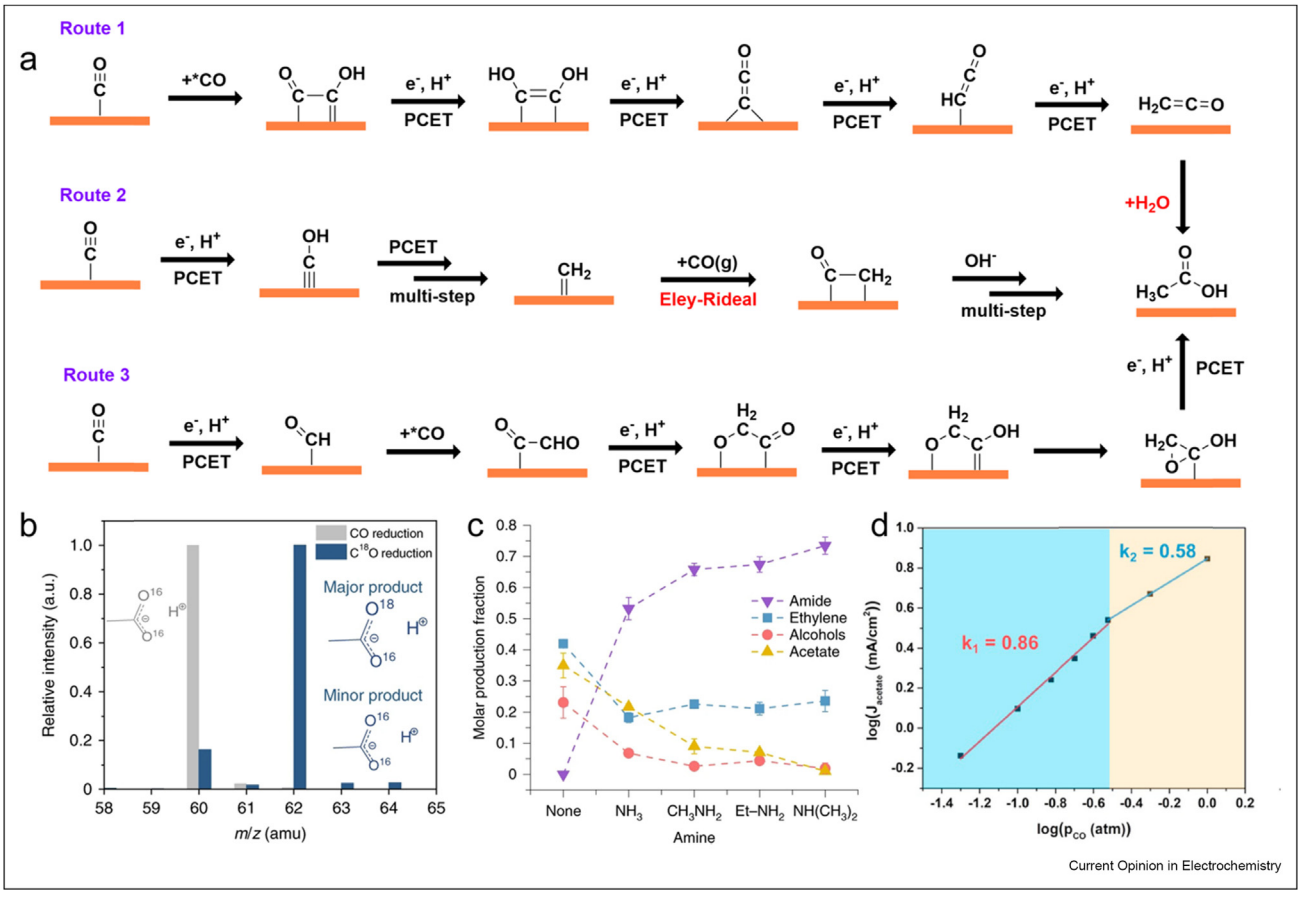

Proposed three reasonable reaction mechanisms for (**a**) the electrocatalytic CORR to acetic acid, path 1: the ethenone mechanism; path 2: the CO insertion mechanism following the Eley-Rideal process; path 3: a three-membered ring intermediate. (**b**) Mass spectrum of partially labeled acetic acid by $C^{18}O$ feedstock on OD-Cu. (**b**) is reproduced from the study by Jouny et al. [76] with the permission from Spring-Nature, copyright 2018. (**c**) Comparison of amide selectivity and other CORR products with the presence of different amine co-feeding operation. (**c**) is reproduced from the study by Jouny et al. [83] with the permission from Spring-Nature, copyright 2019 (**d**) Acetic acid partial current densities over the partial pressure of CO. (**d**) is reproduced from the study by Fu et al. [89] with the permission from Elsevier, copyright 2021.

shows that this mechanism can be extended to other amide formations, and other C_{2+} products are also suppressed in the presence of amines.

Some other reasonable mechanisms may also coexist in the CO-to-acetate process, such as the CO insertion mechanism. This DFT-predicted mechanism is illustrated in Figure 5a (Route 2). Starting from adsorbed *CO, it follows several PCET steps to generate $*CH_2$ species. The generated $*CH_2$ species have a low kinetic barrier for the CO insertion step above Cu sites, and they easily form $*CH_2CO$ [92–94]. The $*CH_2CO$ intermediate was regarded as a precursor for subsequent oriented formation of acetate. There are relatively fewer experimental results of this mechanism. As indicated in Figure 5d, Fu et al. designed a Cu–N–C catalyst for the acetate production [89] and measured the relationship between CO partial pressure and acetate partial current. The results showed that even though the CO partial pressure is adequate to saturate Cu sites, the logarithmic $j_{acetate}$ steadily increases. The result is strong evidence for the Eley-Rideal mechanism in which the rate-determining step (RDS) involves gas CO molecules rather than adsorbed *CO [95]. When the CO partial pressure is sufficiently high, the measured kinetic constant is between the Langmuir–Hinshelwood mechanism and the Eley-Rideal mechanism [95,96]. Meanwhile, the Tafel slope of −118 mV dec^{-1} suggests that the first PCET step is also a slow step. The above information together indicates a mixed RDS including the first PCET step and CO-insertion step.

The third mechanism is rarely reported, but it is reasonable to explain the existence of double-labeled acetic acid ($^{12}CH_3^{12}C^{18}O^{18}OH$) when using $C^{18}O$ feedstock. As shown in Figure 5a (Route 3), Garza et al. proposed that intermediates might form unstable three-membered ring acetolactone species via reduction and

cyclization [88]. Subsequent ring cleavage, reduction, and proton transfer trigger double-labeled acetic acid ($^{12}CH_3^{12}C^{18}O^{18}OH$) formation. Despite its unstable configuration, a trace amount of acetolactone has been detected by mass spectrometry experiments as a transient species [97]. Unfortunately, little other evidence is available to prove this mechanism.

In summary, the major CO-to-acetate mechanism includes: 1) nucleophilic attack on the ethenone intermediate, 2) the three-membered ring mechanism, and 3) the CO-insertion mechanism. It should be noted that the existence of other mechanisms is also possible but still remains controversial. For example, Koper and Birdja proposed that acetate might be generated by a Cannizzaro-type reaction from a key acetaldehyde intermediate [52]. Nevertheless, ethanol formation should also be pH-dependent due to the property of the Cannizzaro-type reaction; this mechanism also expects equal amounts of ethanol and acetate to be distributed in the product [98]. In addition, another work indicated that the potentials required to directly reduce from acetaldehyde are too high (−1.5 to −2.0 V *vs.* RHE) [88], making acetaldehyde path susceptible. Given that the pathway via ethenone is the most reliable route in the CO-to-acetate process, the following discussion for catalyst design would surround Route 1.

Catalyst design for indirect conversion

The Tafel slopes of most CO-to-acetate catalysts are approximately 118 mV dec^{-1} [49,82,99], indicating that the first electron transfer step to CO is the RDS. On the other hand, the key intermediate in CO-to-acetate is ethenone, as discussed in Route 1 (Figure 5a); thus, a special catalyst design is required to decrease the Gibbs energy barrier of *OC-COH to *CCO. Nevertheless, under the guidance of the BEP relationship, catalysts with stronger *CO binding would undesirably lead to increased C—C coupling barriers [93]. Therefore, the optimal catalyst for the CORR toward acetate should exhibit the following factors: proper CO coverage for C—C coupling and rapid electron transfer ability, as well as its ability to break the BEP relationship. In this section, we will discussed the catalyst designs developed in CO-to-acetate process.

Table 2 presents an exhaustive list of the reported catalysts in literature about CO-to-acetate process. The earliest study of CORR can be traced back to the 20th century by Hori et al. [42]. The current density in the initial CORR study was as low as 2.5 mA cm^{-2} over several bulk metal electrodes, including Fe, Ni, and Cu. Surprisingly, only trace amounts of CORR products could be detected on Fe and Ni electrodes, whereas Cu exhibited 60% total FE of mixed products including ethylene, ethanol, and methane. Cu is the only known metal that shows desirable CORR activity toward C_{2+} oxygenate, among which acetic acid is often regarded as a byproduct [64]. Later, OD-Cu was widely applied in the CORR [49,76]. Unlike Cu foil or Cu NPs, OD-Cu contains complex microscopic surface structures (including lattice defects and CuO_x species), which are unstable in monocrystalline Cu electrodes. They discovered that OD-Cu dramatically lowers CO-reduction overpotential compared with Cu foil, together with a much higher CORR FE (Figure 6a). This enhancement was attributed to the highly active twin boundaries formed during the electrochemical reduction [104]. The effects of CuO_x species in the CORR could be excluded by the surface-enhanced Raman spectroscopy [105].

Phase engineering is a pervasive strategy actively studied in CO_2RR [106]. Inspired by this, many works have been devoted to surface engineering on pure Cu catalysts to tune the binding energy of intermediates. For

Table 2

Performance of catalysts investigated for CORR toward acetate.

Catalyst	$FE_{acetate}$ (%)	Total Current density (mA cm^{-2})	Potential (V vs. RHE)	Stability (h)	Reactor	Electrolyte	Reference
OD-Cu	~15	~0.5	−0.30	–	H Cell	0.1M KOH	[49]
micrometre copper	~30	–	−0.70	1	Flow cell	1M KOH	[76]
Cu NS	~48	~200 ($j_{acrtate}$ = 131)	~-0.73	3	Flow cell	2M KOH	[82]
Cu NC (medium)	43	450	~-2.20	150	special cell	PSE	[77]
Cu NW-150	~20	~0.1	−0.25	–	gas-tight cell	0.1M KOH	[100]
GB-Cu	46	~700 ($j_{acrtate}$ = 321)	−0.78	–	Flow cell	1M KOH	[16]
Cu-Pc	36	200	−1.60	20	Flow cell	2M KOH	[101]
Cu−Cu SAC	~30	~110	−1.66	–	Flow cell	0.1M $KHCO_3$	[102]
N−Cu	42	~300 ($j_{acrtate}$ = 180)	−1.27	1	Flow cell	2M KOH	[84]
Cu(I)-benzimidazole	61	400	−0.59	250	Flow cell	3M KOH	[103]
$Cu_{49}Pd_{51}$	>65	>200	−1.00	30	Flow cell	1M KOH	[99]
CuPd	~70	~650 ($j_{acrtate}$ = 425)	−1.03	500	Flow cell	1M KOH	[78]

Figure 6

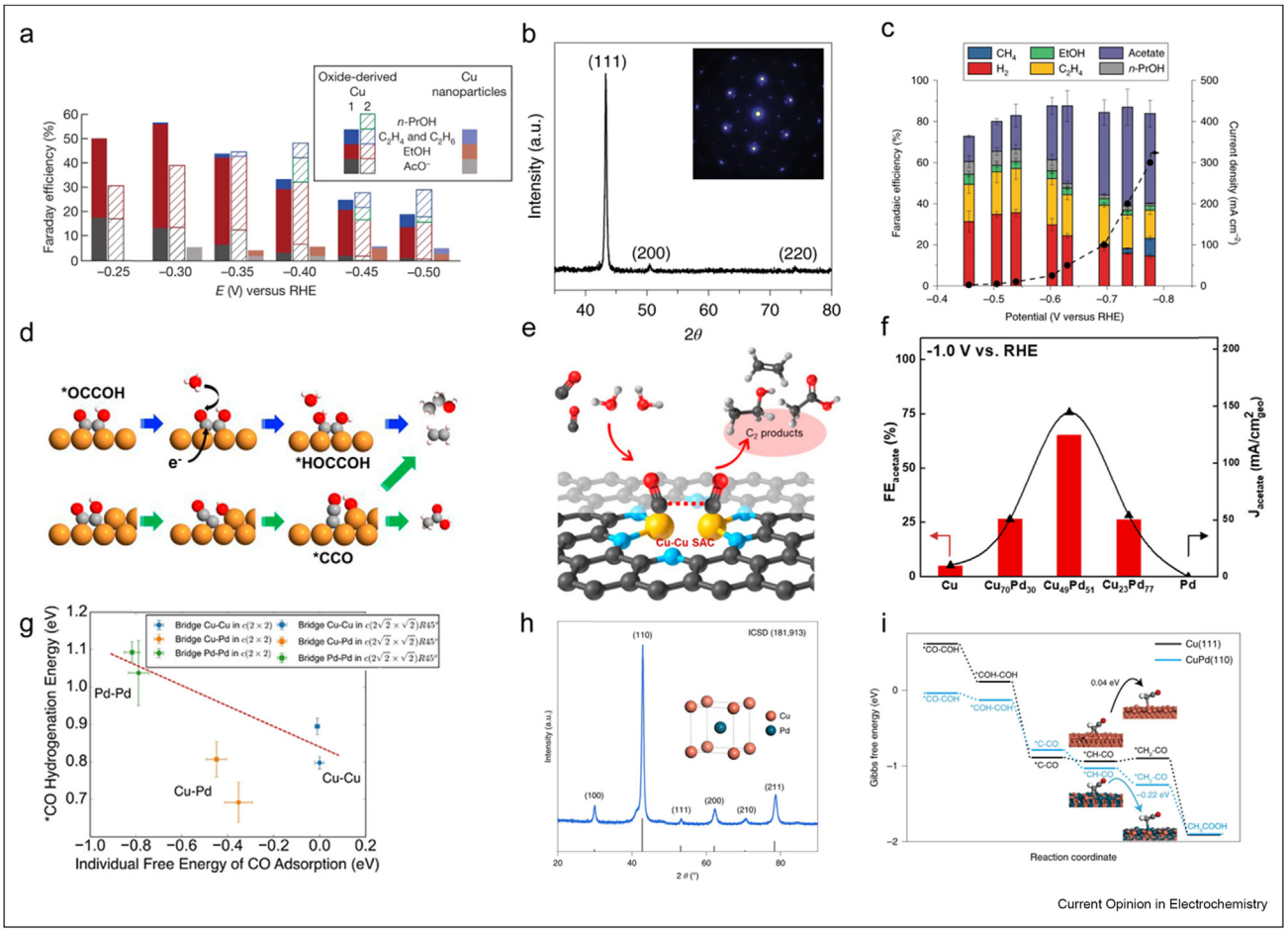

(**a**) FE for CORR product (n-propanol, ethylene, ethane, ethanol, and acetate) distribution at selected potentials (*vs.* RHE). (**b**) XRD and SEAD patterns of Cu nanosheets showing the exposed (111) facets. (**c**) Product distribution among Cu (111) under various applied potentials. (**a–c**) is reproduced from the studies by Li et al., Luc et al. [49,82] with the permission from Spring-Nature, copyright 2014, 2019. (**d**) Distinct CO to C_{2+} route over flat or stepped Cu. The step sites favor the formation of *CCO. Reproduced from the study Zhu et al. [77] with the permission from Proc. Natl. Acad. Sci. U. S. A., copyright 2019. (**e**) Illustration of dual Cu–Cu SAC for CO conversion toward C_{2+} oxygenates (red: oxygen, gray: carbon, yellow: copper, blue: nitrogen, white: hydrogen). Reproduced from the study Li et al. [102] with the permission from American Chemical Society, copyright 2021 (**f**) FE of acetate over PdCu alloys exhibits a "volcano" relationship as Pd content increases. (**g**) The relationship between CO adsorption energies and CO hydrogenation energies over Pd–Cu systems. This result indicates the calculated deviation from the BEP relationship in the Cu–Pd sites. (**f**) and (**g**) are reproduced from the study Shen et al. [99] with the permission from American Chemical Society, copyright 2022. (**h**) XRD patterns of the CuPd intermetallic compound, indicating that the side faces are mainly enclosed by (110) facets. (**i**) Gibbs free energy evolution for acetic acid formation on CuPd (110) compared with Cu (111) at 0 V (versus SHE). (**h**) and (**i**) are reproduced from the study Ji et al. [78] with the permission from Spring-Nature, copyright 2022.

example, Cu nanocrystals exposing different facets have been thoroughly investigated in the CO_2RR and exhibit an apparent facet-dependent selectivity [107]. A similar phenomenon was also observed in the CORR toward acetate. As shown in X-ray diffraction (XRD) and selected area electron diffraction (SEAD) patterns, Cu nanosheets enclosed by {111} facets exhibited 48% acetate FE and a partial current density of 131 mA cm^{-2} (Figure 6b and c) [82]. As a comparison, Cu nanocubes (NCs) orientated in the study by Racit et al. [100] direction were also synthesized to investigate the relationship between selectivity and morphology. According to previous studies, Cu with a high density of (111) suppressed the formation of ethylene and ethanol compared with (100) and (110) [85,108]. However, the intrinsic activity of Cu (111) in the CORR was lower than that of Cu (100). A detailed theoretical explanation is provided by Raciti et al. [100]. Based on their calculations, the CO binding energies over the Cu surface follow (111) < (100) < (110), confirming the lower activity of Cu (111). To improve the intrinsic activity while maintaining acetate selectivity over Cu catalysts, a preliminary study over Cu nanocubes (NCs) with exposed (100) facets reported an acetate FE of 43% and partial current density of approximately 200 mA cm^{-2} [77]. The unique performance of Cu NCs was

attributed to the stepped edge sites, which readily accelerated the dissociation step of *OC-COH to generate *CCO. A thorough DFT calculation in this work predicted that the step defects of high-index surfaces could reduce the *OH dissociation barrier. Compared with the flat Cu surface, the *OCCOH-to-*CCO & *OH dissociation energy barrier over the step defect was found to be 0.38 eV lower (Figure 6d). These results clearly indicated that Cu with grain boundaries and step defects promoted ethenone formation. Inspired by this work, our group recently synthesized a grain-boundary-rich Cu (GB-Cu) catalyst via a pulsed electrochemical reduction process [16]. As expected, the FE of acetate reached 46% at −0.78 V *vs.* RHE under a high partial density of 321 mA cm^{-2}. When the GB-Cu was annealed to reduce defect density, the as-prepared Cu exhibited dramatically lower activity toward acetate. This implies the importance of Cu grain boundaries in breaking the BEP relationship for effective acetate production.

Tuning the electronic structures of metal centers by coordination effect offers another strategy for achieving high CO-to-acetate efficiency. For instance, Fu et al. constructed isolated Cu-N_x sites among Cu−N−C catalysts, achieving 30% FE toward acetate [89]. Distinguished from bulk Cu catalysts, the generation of acetate among Cu-N_x was found to follow the CO insertion mechanism (Route 3, Figure 5a). The absence of Cu−Cu interactions was confirmed in the Fourier transformed extended X-ray absorption fine structure (EXAFS) spectra, indicating that Cu atoms were monodispersed. It was found that CO partial pressure had a greater influence on current density, proving the involvement of direct CO insertion during CORR-to-acetate. A similar observation was also reported for copper phthalocyanine (CuPc) catalysts by Berlinguette et al., [101]. As a result, the total FE of acetate was approximately 70% at 200 mA cm^{-2}, highlighting the extraordinary catalytic efficiency of Cu-N_x sites for acetate production. Similarly, Zheng and cooperators designed a dual single-atom catalyst (Figure 6e) exhibiting an outstanding C_{2+} selectivity (91%). The evidence of Cu−Cu neighboring interaction and the existence of Cu_2N_6 active sites were proved by Cu K-edge EXAFS. DFT calculation indicates N-coordinated adjacent Cu atoms have lower CO dimerization barrier, yielding a significant enhancement of acetate formation [102]. The superior performance of Cu−N coordination bonds is also proposed by Sargent et al. very recently. They anchored Cu(I) over coordination polymer which generate exceptionally stable active sites, characterized by EXAFS. The reported overpotential for 400 mA cm^{-2} operation is only −0.59 V (*vs.* RHE) [103]. Another innovative work was reported by Ni et al. [84]. They synthesized N-modulated Cu catalysts with homogeneously distributed N atoms in the Cu lattice. DFT calculations demonstrated that N-doped Cu^+ sites could promote the *OH dissociation from *OCCOH, resulting in lower formation energy of *CCO species by 0.36 eV compared with the pure Cu catalyst.

From the perspective of tuning electronic properties, creating metal−metal interactions in bimetallic catalysts is another way to stabilize particular intermediates and enhance product selectivity. At present, the Pd−Cu bimetallic system is the only example that has been fully investigated for the CO-to-acetate process. Wang's group designed a series of Cu−Pd alloys with different ratios to study the CORR performance [99]. Specifically, the trend in terms of Pd ratio and acetate FE followed a "volcano" shape (Figure 6f). An asymmetrical C−C coupling mechanism was proposed by the authors to explain the composition-related performance: the adsorbed *CO configuration shifted from the top configuration to bridge configuration when Pd content increased, resulting in a lower *CO hydrogenation barrier toward *CHO. Figure 6g shows the correlation of the *CO hydrogenation energy to the CO adsorption energy over different bimetallic Cu−Pd surfaces, clearly demonstrating the deviation from the BEP relationship over Cu−Pd sites. Finally, they demonstrated that the $Cu_{49}Pd_{51}$ catalyst with a nearly equivalent atom ratio exhibited the highest performance in the CORR toward acetate. Similarly, an ordered PdCu intermetallic compound was successfully synthesized by Zheng group [78]. Structure characterization and DFT calculations suggested that the compound exhibits an ordered body-centered cubic (B2) phase and *CO exhibited a stable triple-bound configuration on $CuPd_2$ hollow sites, leading to the enhancement of *CO coverage (Figure 6h). In addition, the Gibbs free energy of the ethenone formation step was much lower for CuPd than for either Cu or Pd (Figure 6i). As a result, the ordered CuPd catalysts efficiently reduced CO to acetic acid with an unprecedented FE of 70% at a partial current density of 425 mA cm^{-2}. Moreover, CuPd could incessantly operate in MEA for 500 h without appreciable performance decay, resulting in a constant acetate production stream of 1.1 μmol s^{-1} cm^{-2}.

Contrastingly, studies on CORR are relatively fewer than CO_2RR, whereas CORR catalysts generally exhibit higher FE toward acetate. Consequently, numerous number of potential catalysts is pending further exploration. Cu nanocrystals is widely applied for CO-to-acetate process, as well as the undemanding synthesis (compared to those sophisticated ones in CO_2-to-acetate). Many works have verified the grain boundaries above Cu surface contribute to acetate formation, corresponding to the BEP relationship: high selectivity requires asymmetrical active sites to avoid activity scarification. However, acetate selectivity above Cu nanocrystals is limited to be lower than 50%. To date,

Figure 7

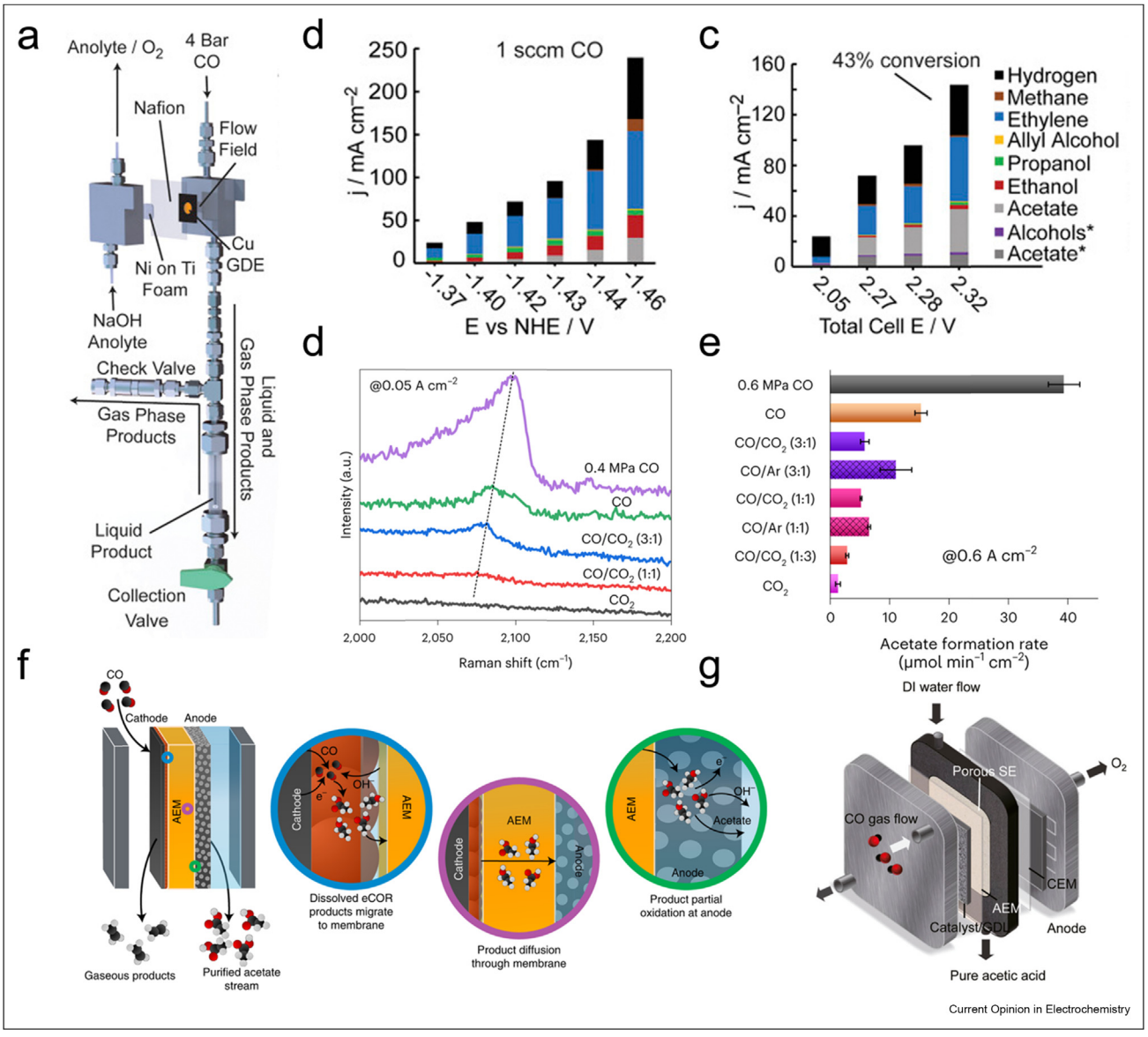

(**a**) CO electrolysis with GDE supplied by interdigitated flow fields in an electrochemical cell for concentrated acetate production. (**b**) Product distribution and applied cathode potentials measured in traditional flow cell with 1 sccm CO flux. When the same process was operated in 4 bar and 1 sccm CO, the product distribution is illustrated in (**c**). The asterisks represent the products collected in anode side. Figure (**a–c**) are reproduced from the study Ripatti et al. [65], with the permission from the Cell Press, copyright 2019. (**d**) Operando CO adsorption Raman peaks among CuO with different feed gas. (**e**) Acetate formation rates measured under different atmosphere at 0.6 A cm^{-2}. Figure (**d**) and (**e**) are reproduced from the study Wei et al. [110], with the permission from the Spring-Nature, copyright 2022. (**f**) Schematic of the CORR electrolyzer design incorporating a permeable AEM to convert ethanol by-product into acetate in anolyte chamber. Figure (**f**) is reproduced from the study Overa et al. [79], with the permission from the Spring-Nature, copyright 2022. (**g**) Schematic illustration of solid electrolyte reactor system to generate pure acetic acid solution stream. Reproduced from the study Zhu et al. [77] with the permission from Proc. Natl. Acad. Sci. U. S. A., copyright 2019.

incorporating Pd element into Cu lattice is proved to be utmost effective in CO-to-acetate process. The proposed PdCu intermetallic compound may inspires following works to apply multi-metallic catalysts. The similarity of Cu-based metallic catalysts is in mechanism. The formation of *H_2CCO intermediates governs high acetate selectivity, which offers us a critical guideline in CO-to-acetate process. Besides, several catalysts composed of isolated Cu sites can also selectively generate acetate, some of which may follow a distinct conversion mechanism via CO insertion (route 2 in Figure 5). Interestingly, most of them consist Cu–N coordination bonds, revealing the design principle of Cu single-atom catalysts.

Non-catalyst parameters for acetate production

Although catalyst designs play an important role in the device performance, some literature exceptionally indicated the microenvironment around the catalytic center may also govern the acetate selectivity. Besides, traditional electrolysis systems applied for $CO_{(2)}RR$ are hard for industrial-scale application. In this section, we briefly summarize the prior non-catalyst techniques reported for acetate efficiency improvement, from the perspective of electrolyte and electrolyzer design.

Modulating electrolytes

It is widely accepted that electrolyte pH dramatically influences acetate selectivity in comparison to ethylene and ethanol [76,98,99,109]. This phenomenon was initially reported by Jiao and cooperators. They conducted CORR in varied concentrations of KOH and found that utmost acetate FE was achieved in highest pH [76]. This phenomenon supports the mechanism that acetate arises from the attack of OH^- on surface-bound intermediates. They further used ab initio calculation to investigate the selectivity determining steps [109]. The result indicated that, though acetate formation did not involve separated RDS from ethylene and ethanol, H_2COO species was effectively removed by OH^- rather than get further reduced among catalyst, promoting acetate selectivity. Hence, it is inexpensive and effective to facilitate acetate formation in virtue of concentrated alkaline media.

Electrolyzer designs

The configuration of electrolyzer determines operation modes in CO_2RR. Traditional H-type cell and flow cell reactors are only qualified for atmospheric pressure, operation in elevated pressure is worth investigation. In 2019, Kanan's group apply pressurized feed gas to CORR electrolyzer [65]. They removed catholyte chamber and introduced interdigitated flow fields into a special MEA reactor which can endured continuous 4 bar CO flow (Figure 7a). Compared with the product distribution in traditional flow cell (Figure 7b), the MEA reactor performed markedly higher acetate selectivity and CO conversion as shown in Figure 7c. Another work published by Wei et al. conducted in-situ experiments to explain the enhancement [110]. As shown in operando Raman (Figure 7d), the peak area of *CO increased with elevated CO pressure, implying the pressurized CO yield higher *CO coverage above catalyst. Meanwhile, they observed obvious peak shifts toward higher wavenumber attributed to distinct CO adsorbed sites. According to the literature, CO peaks in higher wavenumber originates from adsorption over Cu step sites rather than terrace [111]. This result also validates the discussion in Section "Several plausible mechanisms" that Cu step sites prefer *OH dissociation process to generation *COO intermediates (Figure 6d). With theoretical guidance, the performance of CuO nanosheets indeed exhibit higher acetate formation rate under 0.6 MPa CO, as shown in Figure 7e. They further assembled four 100 cm^{-2} MEA for scale-up demonstration. The continuous acetate formation rate achieved 2.97 g min^{-1} at unprecedented 250 A, highlighting the effectiveness of high pressure MEA. Therefore, future work can concentrate on operating the electrolyzer in higher CO pressure to facilitate acetate formation.

Impurity problem should also be surmounted. The key step of CORR to acetate, ethenone formation, and subsequent hydrolysis to acetate, always requires the presence of concentrated hydroxide ions. Thus the generated product is usually contaminated by electrolyte salts (*e.g.*, KOH), even in noncatholyte electrolyzers [65]. On the other hand, the major organic contamination in product stream is ethanol, formate (absence in CORR) and propanol. Given that certain industrial processes require pure acetic acid as feedstock, the energy-intensive downstream separation process will inevitably hamper its commercial applications. Fortunately, several practical solutions have been reported. Firstly, ethanol in product stream can be oxidized into acetate. In term of that, Jiao and his team fully utilized the ethanol permeability property in anion-exchange membrane AEM to eliminate co-existed ethanol [79]. They incorporated an ethanol partial oxidation anode and a well-designed AEM in the CORR electrolyzer, which converted undesirable ethanol into acetate (Figure 7f). Consequently, ultra-pure acetate was obtained with a concentration as high as 7.6 M. Actually, this technique indirectly boosts acetate selectivity, but KOH contamination is not excluded. Another work published by Wang et al. applied PSE into CORR to generate pure acetic acid solution [77]. The model of the special reactor is illustrated in Figure 7g. Without soluble electrolyte, generated acetic acid solution was carried out by pure water to prevent any electrolyte contamination. The output acetic acid solution purity was up to 98 wt% under 150 mA cm^{-2} over 150 h. This system is also suitable for CO_2RR in their early exploration [112,113], in which pure formic acid solution over Bi catalysts and acetic acid solution (also consisted of ethanol and propanol) over Cu catalysts without electrolyte contamination were obtained. In future studies, we can combine the ideas of these works to eliminate both organic and electrolytical impurities in acetic acid stream.

Summary and outlook

Both CO_2RR and CORR are potential routes to restore excess renewable electricity, but they require further improvement in catalyst performance and device scalability. In order to produce profitable chemicals, some vital parameters in CO_xRR should be taken into considerations: activity, selectivity, stability and whole-device energy efficiency. One of the most important

aspects is catalyst design, the point of which is to tune the binding energies of key intermediates to construct a kinetic-favored reaction path. Generally, only Cu-based catalysts can efficiently electrochemically reduce CO_x to C_{2+} oxygenates, but the wide product spectrum leads to additional purification costs. Thus, the modified Cu-based catalysts had been profoundly investigated to break the BEP relationship for high acetate selectivity. At present, two major routes have hitherto been actively studied: i.e., the direct CO_2RR route and the indirect one via CORR. The mechanistic insights based on theoretical calculations and operando experiments can offer valuable information for designing state-of-the-art catalysts.

For the sake of clarity, it is essential to compare the mechanism difference reported in CO_2RR and CORR. Firstly, some CO_2RR mechanisms are ambiguous while the CORR mechanisms are generally clear and convinced. In this review, we summarize four distinct mechanisms in CO_2-to-acetate through totally different intermediates. It can be attributed to the non-unity configurations of catalysts, which may yield ambiguous and versatile results. A variety of catalysts, including mixed-valence Cu [40], single-site catalysts [38], and bimetallic catalysts [36], have been claimed to be effective in the direct CO_2-to-acetate process, with catalyst-dependent reaction mechanisms proposed. Therefore, It is difficult to conclude find out a universal way to manipulate the electronic properties or configurations of the catalyst [33]. On the contrary, most of CORR catalysts share the ethenone species as key intermediate which simplify the obstacle to study this reaction. Based on the analogical mechanism, many universal strategies have been applied to enhance CO-to-acetate selectivity: using high-pH electrolyte, constructing catalysts with step sites and elevating *CO coverage, etc. Additionally, the intrinsic difference in *CO coverage results in diverged conversion routes. As shown in route 1 of Figure 2 and route 1 of Figure 5, though ethenone-path is claimed to be possible in the evolution of adsorbed *CO, few reports have directly observed the existence of ethenone in CO_2-to-acetate. This phenomenon may be the result of inadequate *CO coverage in CO_2RR [109]. Besides, as shown in route 2 of Figure 2 and route 3 of Figure 5, although some common intermediates (*CHO) may exist in both CO_2RR and CORR, further conversion exhibit distinct path due to different *CO coverage. In this way, even the same catalysts may exhibit different product distribution in CO_2 feed compared with CO feed. Finally, whether acetate originates from acetaldehyde disproportionation in particular route is controversial in both CO_2RR and CORR. Although Koper et al. conducted thorough experiments to prove the viability of this mechanism [52], Jiao and cooperators pointed out that it would yield pH-dependent ethanol formation and equal amount of acetate and ethanol [109]. This mechanism should be further investigated with adequate experiments and calculations in the future. Some similarities between CO_2RR and CORR also deserve discussion. Firstly, for catalysts with isolated sites, both CO_2RR and CORR may involve Eley-Rideal process. Thus, elevating CO_2 or CO partial pressure would accelerate acetate formation rate in these catalysts. Secondly, for Cu based catalysts, both CO_2RR and CORR may involve *CO dimerization step. Introducing other elements to increasing *CO coverage among Cu surface is a universal strategy. The $(Cu)_n$, $(Ag)_m$ tandem catalyst is a good example [36]: the presence of Ag increasing CO concentration around Cu sites, which is similar to direct use CO feed to undergo CO-to-acetate process.

Some obstacles may impede the commercialization of electrochemical acetate production. How to handle compatibility problems of the CO_2-to-CO process and the CO-to-acetate process is challenging and rarely reported. Several emergent techniques can be considered for reference, but still exist intrinsic shortcomings. Firstly, perhaps CO_2RR and CORR processes coexisted compatibility in the design of tandem catalysts, the intrinsic CO_2 carbon loss during CO_2RR is still a daunting task in alkaline media. On the other hand, two components in the tandem catalyst may interfere with each other, leading to undesirable performance. Another alternative strategy is called the two-step electrolysis. Specifically, catalysts are placed into two separate electrochemical cells with distinct optimum electrolytes. A good example in the literature has been reported by Sargent's group. They designed a long-term ethylene oxide production system via two separated cells in series [114]. The two-procedure CO_2-to-acetate may also be applicable and have other benefits: the CO_2-to-CO catalyst can work under a non-alkaline electrolyte to avoid carbon loss, while the alkaline electrolyte in the second cell accelerates the CORR process. Our group recently also showed the feasibility of producing pure acetic acid solution via a two-step CO_2 electrolysis [16]. However, the purity of the output CO gas stream in CO_2-to-CO is strictly needed, since unconverted CO_2 gas would dilute the CO concentration resulting product distribution aberration, as predicted by several works [76,115]. In this way, future works should focus on improving CO_2 single-pass conversion. Recent work also reported the improved ethylene formation efficiency under CO_2—CO co-feeds [110,116], which may offer worthy insights for CO electrolysis with mixed CO_2 feeds. In addition, the operation in large current densities would lead to an undesired high overpotential and cause extra cost due to the wasted energy. In this regard, the industrial-scale production of acetate or acetic acid through CO_2 electrolysis is still a challenging task. Except for the catalyst itself, few CORR studies have been conducted on the engineering part of the whole device. Future investigations can be devoted to seeking matched ion-exchange membranes, electrolyzer

designs, and rationally designed integrated and compact electrolysis systems for efficient acetate production.

CO_2 electrolysis technique toward acetate (acetic acid) production provides appealing prospects for recycling greenhouse gas emissions into profitable chemicals. And it is possible to provide a platform for developing electricity-driven manufacturing factories. For extensive implementation, it is attractive to further upgrade acetate and acetic acid to more valuable chemicals. Some transformative approaches should be taken into consideration in future works. (1) Co-electrolysis technique is proposed to directly generate acetate derivatives from CO. For example, NH_3—CO co-feeds are successfully demonstrated to promote various amide formation [83], ingeniously inspired from the route 1 in Figure 5. This discovery triggered the extension to other nucleophilic agents. Zhou et al. conducted CORR in the presence of alkyl alcohol compounds. Initially, a series of C_3—C_6 acetate esters were directly obtained in MEA cells with a partial current density up to 55 mA cm^{-2} [117]. Consequently, co-electrolysis would broaden the viable products spectrum in CO_xRR electrolysis. Some other vital chemicals in acetate-related industrial chain are potential candidates for future exploration, such as acetic anhydride, acetyl chloride, chloroacetic acid and vinyl acetate, etc. (2) Electrifying biosynthesis is an appealing blue ocean. Although the reported CO_2RR product spectrum is always confined to short-chain organic chemicals, the combination with biological synthesis shows a promising strategy to expand the product portfolio. Acetate is a competitive energy carrier that can be metabolized by a wide array of microorganisms. And techniques in acetic acid production have been successfully operated compatibly with biosynthesis system. For example, our group designed an electrobiocatalysis hybrid system that continuously converted CO_2 to acetic acid; the obtained acetic acid was directly used as feedstock for microbes to produce glucose and fatty acids [16]. Similarly, Hann et al. designed a novel system to directly cultivate food organisms in acetate streams from CO_2 electrolysis [118]. The proper acetate and electrolytes ratio was necessary to support biological growth. They successfully grew heterotrophic algae, fungi, and crop plants, suggesting the possibility to cultivate food without photosynthesis process. These works independently optimized electrochemical and microbial processes and then coupled, which overcome the interference between electrodes and microbe in direct bio-electrosynthesis [119]. Other advantages for introducing acetate into microbial synthesis rather than directly utilize CO_2/CO or other C_1/C_2 molecules are obvious: acetate is soluble in aqueous phase while gaseous CO_2 and CO suffer from intrinsic mass transfer problem constraining scalability. Besides, acetate is biocompatible compared to ethanol, methanol and formic acid lessening the death of microbes. To further put forward large-scale electrifying biosynthesis, the acetic acid produced from the electrolysis process should be concentrated and nontoxic which can be directly consumed by microbes to efficiently produce long-chain chemicals.

Given the bright prospect of an electricity-driven acetate industry, fundamental technological advances are still relying on acetate production efficiency, which require intensive efforts for CO_2RR and CORR in various aspects: activity, selectivity, stability, product purity, and the coupling of different electrocatalytic processes.

Declaration of competing interest

The authors declare that they have no known competing financial interests or personal relationships that could have appeared to influence the work reported in this paper.

Data availability

No data was used for the research described in the article.

Acknowledgments

C.X. acknowledges the National Natural Science Foundation of China (NSFC 22102018 and 52171201), the Natural Science Foundation of Sichuan Province (2022NSFSC0194), the "Pioneer" and "Leading Goose" R&D Program of Zhejiang (No. 2023C03017), the Hefei National Research Center for Physical Sciences at the Microscale (KF2021005), and the University of Electronic Science and Technology of China for startup funding (A1098531023601264). Q.J. acknowledges the China Postdoctoral Science Foundation funded project (2022M710601) and the University of Electronic Science and Technology of China for startup funding (Y030212059003039). T.Z. acknowledges the NSFC (22005291 and 22278067) and University of Electronic Science and Technology of China for startup funding (A1098531023601356).

References

Papers of particular interest, published within the period of review, have been highlighted as:

* of special interest
** of outstanding interest

1. Solomon S, Plattner GK, Knutti R, Friedlingstein P: **Irreversible climate change due to carbon dioxide emissions**. *Proc Nat Acad Sci USA* 2009, **106**:1704–1709.

2. Acosta-Silva YD, Torres-Pacheco T, Matsumoto Y, Toledano-Ayala M, Soto-Zarazua GM, Zelaya-Angel O, Mendez-Lopez A: **Applications of solar and wind renewable energy in agriculture: a review**. *Sci Prog* 2019, **102**:127–140.

3. Khare V, Nema S, Baredar P: **Solar-wind hybrid renewable energy system: a review**. *Renew Sustain Energy Rev* 2016, **58**: 23–33.

4. Bushuyev OS, De Luna P, Dinh CT, Tao L, Saur G, van de Lagemaat J, Kelley SO, Sargent EH: **What should we make with CO2 and how can we make it?** *Joule* 2018, **2**:825–832.

5. Jouny M, Luc W, Jiao F: **General techno-economic analysis of CO_2 electrolysis systems**. *Ind Eng Chem Res* 2018, **57**: 2165–2177.

6. Shin H, Hansen KU, Jiao F: **Techno-economic assessment of low-temperature carbon dioxide electrolysis**. *Nat Sustain* 2021, **4**:911–919.

7. Jin S, Hao ZM, Zhang K, Yan ZH, Chen J: **Advances and challenges for the electrochemical reduction of CO_2 to CO: from fundamentals to industrialization**. *Angew Chem Int Ed* 2021, **60**:20627–20648.

8. Zheng TT, Jiang K, Ta N, Hu YF, Zeng J, Liu JY, Wang HT: **Large-scale and highly selective CO_2 electrocatalytic reduction on nickel single-atom catalyst**. *Joule* 2019, **3**: 265–278.

9. Han N, Ding P, He L, Li YY, Li YG: **Promises of main group metal-based nanostructured materials for electrochemical CO_2 reduction to formate**. *Adv Energy Mater* 2020, **10**, 1902338.

10. Zheng TT, Liu CX, Guo CX, Zhang ML, Li X, Jiang Q, Xue WQ, Li HL, Li AW, Pao CW, *et al.*: **Copper-catalysed exclusive CO_2 to pure formic acid conversion via single-atom alloying**. *Nat Nanotechnol* 2021, **16**:1386–1394.

11. Yoneda N, Kusano S, Yasui M, Pujado P, Wilcher S: **Recent advances in processes and catalysts for the production of acetic acid**. *Appl Catal A General* 2001, **221**:253–265.

12. Duarte NG, de Queiroz DS, Veloso CdO, de Castro AM, Pereira Langone MA: **Effects of acetic acid addition methods on butyl acetate enzymatic synthesis**. *Chem Eng Commun* 2020, **207**: 177–184.

13. Majzoobi M, Kaveh Z, Farahnaky A: **Effect of acetic acid on physical properties of pregelatinized wheat and corn starch gels**. *Food Chem* 2016, **196**:720–725.

14. Augustine R, Kalarikkal N, Thomas S: **Clogging-free electrospinning of polycaprolactone using acetic acid/acetone mixture**. *Polym-Plast Technol Eng* 2016, **55**:518–529.

15. Huang B, Yang H, Fang GC, Zhang X, Wu H, Li ZM, Ye Q: **Central pathway engineering for enhanced succinate biosynthesis from acetate in Escherichia coli**. *Biotechnol Bioeng* 2018, **115**:943–954.

16. ** Zheng TT, Zhang ML, Wu LH, Guo SY, Liu XJ, Zhao JK, Xue WQ, Li JW, Liu CX, Li X, *et al.*: **Upcycling CO_2 into energy-rich long-chain compounds via electrochemical and metabolic engineering**. *Nat Catal* 2022, **5**:388–396.
This work gives inovative idea to convert CO_2 into glocuse and fatty acid by electrobiocatalysis hybrid system. The obtained acetic acid solution can be directly used as feedstock for microbes to produce long-chain products.

17. Zhang SS, Yang W, Chen H, Liu B, Lin BX, Tao Y: **Metabolic engineering for efficient supply of acetyl-CoA from different carbon sources in Escherichia coli**. *Microb Cell Factories* 2019, **18**:130.

18. Chang ZS, Dai W, Mao YF, Cui ZZ, Zhang ZD, Wang ZW, Ma HW, Chen T: **Enhanced 3-hydroxypropionic acid production from acetate via the malonyl-CoA pathway in corynebacterium glutamicum**. *Front Bioeng Biotechnol* 2022, **9**, 808258.

19. Dimian AC, Kiss AA: **Novel energy efficient process for acetic acid production by methanol carbonylation**. *Chem Eng Res Des* 2020, **159**:1–12.

20. Chu S, Cui Y, Liu N: **The path towards sustainable energy**. *Nat Mater* 2017, **16**:16–22.

21. Guo CY, Guo YH, Shi YM, Lan XN, Wang YT, Yu YF, Zhang B: **Electrocatalytic reduction of CO_2 to ethanol at close to theoretical potential via engineering abundant electron-donating Cu^{0+} species**. *Angewandte Chemie-International Edition* 2022, **61**, e202205909.

22. Ma WC, Xie SJ, Liu TT, Fan QY, Ye JY, Sun FF, Jiang Z, Zhang QH, Cheng J, Wang Y: **Electrocatalytic reduction of CO_2 to ethylene and ethanol through hydrogen-assisted C-C coupling over fluorine-modified copper**. *Nat Catal* 2020, **3**: 478–487.

23. Xie Y, Ou PF, Wang X, Xu ZY, Li YC, Wang ZY, Huang JE, Wicks J, McCallum C, Wang N, *et al.*: **High carbon utilization in CO_2 reduction to multi-carbon products in acidic media**. *Nat Catal* 2022, **5**:564–570.

24. Xu HP, Rebollar D, He HY, Chong LN, Liu YZ, Liu C, Sun CJ, Li T, Muntean JV, Winans RE, *et al.*: **Highly selective electrocatalytic CO_2 reduction to ethanol by metallic clusters dynamically formed from atomically dispersed copper**. *Nat Energy* 2020, **5**:623–632.

25. Nitopi S, Bertheussen E, Scott SB, Liu XY, Engstfeld AK, Horch S, Seger B, Stephens IEL, Chan K, Hahn C, *et al.*: **Progress and perspectives of electrochemical CO_2 reduction on copper in aqueous electrolyte**. *Chem Rev* 2019, **119**:7610–7672.

26. Li K, Peng B, Peng T: **Recent advances in heterogeneous photocatalytic CO_2 conversion to solar fuels**. *ACS Catal* 2016, **6**:7485–7527.

27. Birdja YY, Perez-Gallent E, Figueiredo MC, Gottle AJ, Calle-Vallejo F, Koper MTM: **Advances and challenges in understanding the electrocatalytic conversion of carbon dioxide to fuels**. *Nat Energy* 2019, **4**:732–745.

28. Morales-Guio CG, Cave ER, Nitopi SA, Feaster JT, Wang L, Kuhl KP, Jackson A, Johnson NC, Abram DN, Hatsukade T, *et al.*: **Improved CO_2 reduction activity towards C_{2+} alcohols on a tandem gold on copper electrocatalyst**. *Nat Catal* 2018, **1**: 764–771.

29. Wang G, Chen J, Ding Y, Cai P, Yi L, Li Y, Tu C, Hou Y, Wen Z, Dai L: **Electrocatalysis for CO_2 conversion: from fundamentals to value-added products**. *Chem Soc Rev* 2021, **50**: 4993–5061.

30. Mehta P, Barboun P, Herrera FA, Kim J, Rumbach P, Go DB, Hicks JC, Schneider WF: **Overcoming ammonia synthesis scaling relations with plasma-enabled catalysis**. *Nat Catal* 2018, **1**:269–275.

31. Abild-Pedersen F, Greeley J, Studt F, Rossmeisl J, Munter TR, Moses PG, Skulason E, Bligaard T, Norskov JK: **Scaling properties of adsorption energies for hydrogen-containing molecules on transition-metal surfaces**. *Phys Rev Lett* 2007, **99**, 016105.

32. Bligaard T, Norskov JK, Dahl S, Matthiesen J, Christensen CH, Sehested J: **The Bronsted-Evans-Polanyi relation and the volcano curve in heterogeneous catalysis**. *J Catal* 2004, **224**: 206–217.

33. ** Liu YM, Chen S, Quan X, Yu HT: **Efficient electrochemical reduction of carbon dioxide to acetate on nitrogen-doped nanodiamond**. *J Am Chem Soc* 2015, **137**:11631–11636.
The first reported catalysts which can efficiently convert CO_2 into acetate via an oxalate intermediates. N atoms was doped in diamond nanoarray with sp^3 configuration resulting the special performance.

34. Serafini M, Mariani F, Fasolini A, Scavetta E, Basile F, Tonelli D: **Nanostructured copper-based electrodes electrochemically synthesized on a carbonaceous gas diffusion membrane with catalytic activity for the electroreduction of CO_2**. *ACS Appl Mater Interfaces* 2021, **13**:57451–57461.

35. Lum Y, Ager JW: **Evidence for product-specific active sites on oxide-derived Cu catalysts for electrochemical CO_2 reduction**. *Nat Catal* 2019, **2**:86–93.

36. * Wang Y, Wang DG, Dares CJ, Marquard SL, Sheridan MV, Meyer TJ: **CO_2 reduction to acetate in mixtures of ultrasmall $(Cu)_{(n)}$,$(Ag)_{(m)}$ bimetallic nanoparticles**. *Proc Nat Acad Sci USA* 2018, **115**:278–283.
The as-synthesized Cu and Ag ultra-small nanoparticles was used as tandem catalysts to convert CO_2 into acetate. The Ag provide surface *CO species and Cu sites further conduct C–C coupling.

37. Qiu X-F, Huang J-R, Yu C, Zhao Z-H, Zhu H-L, Ke Z, Liao P-Q, Chen X-M: **A stable and conductive covalent organic framework with isolated active sites for highly selective electroreduction of carbon dioxide to acetate**. *Angew Chem Int Ed* 2022, **61**, e202206470.

38. De RN, Gonglach S, Paul S, Haas M, Sreejith SS, Gerschel P, Apfel UP, Vuong TH, Rabeah J, Roy S, *et al.*: **Electrocatalytic reduction of CO_2 to acetic acid by a molecular manganese corrole complex**. *Angew Chem Int Ed* 2020, **59**:10527–10534.

39. Gonglach S, Paul S, Haas M, Pillwein F, Sreejith SS, Barman S, De R, Mullegger S, Gerschel P, Apfel UP, *et al.*: **Molecular cobalt corrole complex for the heterogeneous electrocatalytic reduction of carbon dioxide**. *Nat Commun* 2019, **10**:1–10.

40. * Zhu QG, Sun XF, Yang DX, Ma J, Kang XC, Zheng LR, Zhang J, Wu ZH, Han BX: **Carbon dioxide electroreduction to C_2**

products over copper-cuprous oxide derived from electrosynthesized copper complex. *Nat Commun* 2019, **10**:1–11.
This research designed a Cu-based catalysts with surfficient Cu–Cu + sites, which was proved as the effecitve CO dimerization site to generate C2+ products.

41. Hara K, Tsuneto A, Kudo A, Sakata T: **Electrochemical reduction OF CO_2 ON a CU electrode under high-pressure - factors that determine the product selectivity**. *J Electrochem Soc* 1994, **141**:2097–2103.

42. Hori Y, Takahashi R, Yoshinami Y, Murata A: **Electrochemical reduction of CO at a copper electrode**. *J Phys Chem B* 1997, **101**:7075–7081.

43. Zhu HL, Chen HY, Han YX, Zhao ZH, Liao PQ, Chen XM: **A porous p-p stacking framework with dicopper(I) sites and adjacent proton relays for electroreduction of CO_2 to C_{2+} products**. *J Am Chem Soc* 2022, **144**:13319–13326.

44. Li HF, Liu TF, Wei PF, Lin L, Gao DF, Wang GX, Bao XH: **High-rate CO_2 electroreduction to C_{2+} products over a copper-copper iodide catalyst**. *Angew Chem Int Ed* 2021, **60**:14329–14333.

45. Zang DJ, Li Q, Dai GY, Zeng MY, Huang YC, Wei YG: **Interface engineering of Mo_8/Cu heterostructures toward highly selective electrochemical reduction of carbon dioxide into acetate**. *Appl Catal B Environ* 2021, **281**, 119426.

46. Genovese C, Ampelli C, Perathoner S, Centi G: **Mechanism of C-C bond formation in the electrocatalytic reduction of CO_2 to acetic acid. A challenging reaction to use renewable energy with chemistry**. *Green Chem* 2017, **19**:2406–2415.

47. Kuhl KP, Cave ER, Abram DN, Jaramillo TF: **New insights into the electrochemical reduction of carbon dioxide on metallic copper surfaces**. *Energy Environ Sci* 2012, **5**:7050–7059.

48. Sun S, Watanabe M, Wu J, An Q, Ishihara T: **Ultrathin WO_3·0.33H_2O nanotubes for CO_2 photoreduction to acetate with high selectivity**. *J Am Chem Soc* 2018, **140**:6474–6482.

49. ** Li CW, Ciston J, Kanan MW: **Electroreduction of carbon monoxide to liquid fuel on oxide-derived nanocrystalline copper**. *Nature* 2014, **508**:504–507.
This work provides an early research toward CO electroreduction reaction for C_{2+} oxygenates formation. The OD-Cu was initially investigated as active catalysts in CO electrolysis. Moreover, it hypothesized surface-bound specied might react with solvent molecules. This work provides critical inspiration for subsequent studies in CO-to-acetate.

50. Cook J, Hamlin JE, Nutton A, Maitlis PM: **Homogeneously catalyzed disproportionation of acetaldehyde into ethanol and acetic-acid**. *J Chem Soc, Chem Commun* 1980:144–145.

51. Nagai Y, Morooka S, Matubayasi N, Nakahara M: **Mechanisms and kinetics of acetaldehyde reaction in supercritical water: noncatalytic disproportionation, condensation, and decarbonylation**. *J Phys Chem A* 2004, **108**:11635–11643.

52. Birdja YY, Koper MTM: **The importance of cannizzaro-type reactions during electrocatalytic reduction of carbon dioxide**. *J Am Chem Soc* 2017, **139**:2030–2034.

53. Xiao H, Goddard WA, Cheng T, Liu Y: **Cu metal embedded in oxidized matrix catalyst to promote CO_2 activation and CO dimerization for electrochemical reduction of CO_2**. *Proceedings of the National Academy of Sciences of the United States of America* 2017, **114**:6685–6688.

54. Lum Y, Ager JW: **Sequential catalysis controls selectivity in electrochemical CO_2 reduction on Cu**. *Energy Environ Sci* 2018, **11**:2935–2944.

55. Cao B, Li F-Z, Gu J: **Designing Cu-based tandem catalysts for CO_2 electroreduction based on mass transport of CO intermediate**. *ACS Catal* 2022, **12**:9735–9752.

56. She XJ, Zhang TY, Li ZY, Li HM, Xu H, Wu JJ: **Tandem electrodes for carbon dioxide reduction into C_{2+} products at simultaneously high production efficiency and rate**. *Cell Reports Physical Science* 2020, **1**, 100051.

57. Zhong YZ, Kong XD, Song ZM, Liu Y, Peng LP, Zhang L, Luo X, Zeng J, Geng ZG: **Adjusting local CO confinement in porous-shell Ag@Cu catalysts for enhancing C-C coupling toward CO_2 eletroreduction**. *Nano Lett* 2022, **22**:2554–2560.

58. Choukroun D, Daems N, Kenis T, Van Everbroeck T, Hereijgers J, Altantzis T, Bals S, Cool P, Breugelmans T: **Bifunctional nickel–nitrogen-doped-carbon-supported copper electrocatalyst for CO_2 reduction**. *J Phys Chem C* 2020, **124**:1369–1381.

59. Dinh CT, Burdyny T, Kibria MG, Seifitokaldani A, Gabardo CM, de Arquer FPG, Kiani A, Edwards JP, De Luna P, Bushuyev OS, *et al.*: **CO_2 electroreduction to ethylene via hydroxide-mediated copper catalysis at an abrupt interface**. *Science* 2018, **360**:783–787.

60. Endrodi B, Samu A, Kecsenovity E, Halmagyi T, Sebok D, Janaky C: **Operando cathode activation with alkali metal cations for high current density operation of water-fed zero-gap carbon dioxide electrolysers**. *Nat Energy* 2021, **6**:439–448.

61. Kim JY, Zhu P, Chen FY, Wu ZY, Cullen DA, Wang HT: **Recovering carbon losses in CO_2 electrolysis using a solid electrolyte reactor**. *Nat Catal* 2022, **5**:288–299.

62. Ooka H, Figueiredo MC, Koper MTM: **Competition between hydrogen evolution and carbon dioxide reduction on copper electrodes in mildly acidic media**. *Langmuir* 2017, **33**:9307–9313.

63. Nitopi S, Bertheussen E, Scott SB, Liu X, Engstfeld AK, Horch S, Seger B, Stephens IEL, Chan K, Hahn C, *et al.*: **Progress and perspectives of electrochemical CO_2 reduction on copper in aqueous electrolyte**. *Chem Rev* 2019, **119**:7610–7672.

64. * Ma WC, He XY, Wang W, Xie SJ, Zhang QH, Wang Y: **Electrocatalytic reduction of CO_2 and CO to multi-carbon compounds over Cu-based catalysts**. *Chem Soc Rev* 2021, **50**:12897–12914.
This review provides worthy remarks towards the relationship between CO_2RR and CORR. The advantages and disadvantages of CO_2RR and CORR are illustrated in details.

65. Ripatti DS, Veltman TR, Kanan MW: **Carbon monoxide gas diffusion electrolysis that produces concentrated C_2 products with high single-pass conversion**. *Joule* 2019, **3**:240–256.

66. Fang M, Xu L, Zhang H, Zhu Y, Wong W-Y: **Metalloporphyrin-linked mercurated graphynes for ultrastable CO_2 electroreduction to CO with nearly 100% selectivity at a current density of 1.2 A cm^{-2}**. *J Am Chem Soc* 2022, **144**:15143–15154.

67. Sheng X, Ge W, Jiang H, Li C: **Engineering the Ni-N-C catalyst microenvironment enabling CO_2 electroreduction with nearly 100% CO selectivity in acid**. *Adv Mater* 2022. e2201295-e2201295.

68. Endrodi B, Kecsenovity E, Samu A, Darvas F, Jones RV, Torok V, Danyi A, Janaky C: **Multilayer electrolyzer stack converts carbon dioxide to gas products at high pressure with high efficiency**. *ACS Energy Lett* 2019, **4**:1770–1777.

69. Li M, Wang H, Luo W, Sherrell PC, Chen J, Yang J: **Heterogeneous single-atom catalysts for electrochemical CO_2 reduction reaction**. *Adv Mater* 2020, **32**, 2001848.

70. Jin S, Hao Z, Zhang K, Yan Z, Chen J: **Advances and challenges for the electrochemical reduction of CO_2 to CO: from fundamentals to industrialization**. *Angewandte Chemie-International Edition* 2021, **60**:20627–20648.

71. Nguyen DLT, Kim Y, Hwang YJ, Won DH: **Progress in development of electrocatalyst for CO_2 conversion to selective CO production**. *Carbon energy* 2020, **2**:72–98.

72. Xu C, Vasileff A, Zheng Y, Qiao S-Z: **Recent progress of 3d transition metal single-atom catalysts for electrochemical CO_2 reduction**. *Adv Mater Interfac* 2021, **8**, 2001904.

73. Yadav DK, Singh DK, Ganesan V: **Recent strategy(ies) for the electrocatalytic reduction of CO_2: Ni single-atom catalysts for the selective electrochemical formation of CO in aqueous electrolytes**. *Curr Opin Electrochem* 2020, **22**:87–93.

74. Guo H, Si D-H, Zhu H-J, Li Q-X, Huang Y-B, Cao R: **Ni single-atom sites supported on carbon aerogel for highly efficient**

electroreduction of carbon dioxide with industrial current densities. *eScience* 2022, **2**:295–303.

75. Li J, Zeng H, Dong X, Ding Y, Hu S, Zhang R, Dai Y, Cui P, Xiao Z, Zhao D, *et al.*: **Selective CO_2 electrolysis to CO using isolated antimony alloyed copper**. *Nat Commun* 2023, **14**:340.

76. * ouny M, Luc W, Jiao F: **High-rate electroreduction of carbon monoxide to multi-carbon products**. *Nature Catalysis* 2018, **1**: 748–755.
This research firstly apply GDE into CORR system to achieve unprecedented current density. Further studies indicated that the most critical challenge to achieve high current density in CO/CO_2 electrolysis is to maintain the effectiveness of the three-phase boundary at the electrode/electrode interface.

77. ** Zhu P, Xia C, Liu CY, Jiang K, Gao GH, Zhang X, Xia Y, Lei YJ, Alshareef HN, Senftle TP, *et al.*: **Direct and continuous generation of pure acetic acid solutions via electrocatalytic carbon monoxide reduction**. *Proc Nat Acad Sci USA* 2021, **118**, e2010868118.
This work developed a porous solid electrolyte to avoid eletrolytes contamination. The upgrading cell produced a 0.33 M acetic acid without any impurity ions, which can be directly put into use for further application.

78. ** Ji YL, Chen Z, Wei RL, Yang C, Wang YH, Xu J, Zhang H, Guan AX, Chen JT, Sham TK, *et al.*: **Selective CO-to-acetate electroreduction via intermediate adsorption tuning on ordered Cu-Pd sites**. *Nat Catal* 2022, **5**:251–258.
The as synthesized CuPd intermetallic compounds have superior performance in CORR to acetate over other reported catalysts. It exhibited the highest acetate FE and long-term stability in 500 mA cm^{-2}. The activity was attributed to the ordered Pd–Cu sites.

79. Overa S, Crandall BS, Shrimant B, Tian D, Ko BH, Shin H, Bae C, Jiao F: **Enhancing acetate selectivity by coupling anodic oxidation to carbon monoxide electroreduction**. *Nature Catalysis* 2022, **5**:738–745.

80. Martín AJ, Larrazábal GO, Pérez-Ramírez J: **Towards sustainable fuels and chemicals through the electrochemical reduction of CO_2: lessons from water electrolysis**. *Green Chem* 2015, **17**:5114–5130.

81. De Luna P, Hahn C, Higgins D, Jaffer SA, Jaramillo TF, Sargent EH: **What would it take for renewably powered electrosynthesis to displace petrochemical processes?** *Science* 2019, **364**. eaav3506.

82. * Luc W, Fu XB, Shi JJ, Lv JJ, Jouny M, Ko BH, Xu YB, Tu Q, Hu XB, Wu JS, *et al.*: **Two-dimensional copper nanosheets for electrochemical reduction of carbon monoxide to acetate**. *Nat Catal* 2019, **2**:423–430.
This work provide an efficient CORR-to-acetate catalysts with the combination of controllable synthesis. The Cu(111) facets were proved to be effective for acetate generation. The key intermediates in this process was proved to be ethenone.

83. Jouny M, Lv JJ, Cheng T, Ko BH, Zhu JJ, Goddard WA, Jiao F: **Formation of carbon-nitrogen bonds in carbon monoxide electrolysis**. *Nat Chem* 2019, **11**:846–851.

84. Ni F, Yang H, Wen Y, Bai H, Zhang L, Cui C, Li S, He S, Cheng T, Zhang B, *et al.*: **N-modulated Cu^+ for efficient electrochemical carbon monoxide reduction to acetate**. *Science China-Materials* 2020, **63**:2606–2612.

85. Calle-Vallejo F, Koper MTM: **Theoretical considerations on the electroreduction of CO to C_2 species on Cu(100) electrodes**. *Angew Chem Int Ed* 2013, **52**:7282–7285.

86. Perez-Gallent E, Figueiredo MC, Calle-Vallejo F, Koper MTM: **Spectroscopic observation of a hydrogenated CO dimer intermediate during CO reduction on Cu(100) electrodes**. *Angew Chem Int Ed* 2017, **56**:3621–3624.

87. Zheng Y, Vasileff A, Zhou X, Jiao Y, Jaroniec M, Qiao S-Z: **Understanding the roadmap for electrochemical reduction of CO_2 to multi-carbon oxygenates and hydrocarbons on copper-based catalysts**. *J Am Chem Soc* 2019, **141**: 7646–7659.

88. Garza AJ, Bell AT, Head-Gordon M: **Mechanism of CO_2 reduction at copper surfaces: pathways to C_2 products**. *ACS Catal* 2018, **8**:1490–1499.

89. Fu X, Wang Y, Shen H, Yu Y, Xu F, Zhou G, Xie W, Qin R, Dun C, Pao CW, *et al.*: **Chemical upgrade of carbon monoxide to acetate on an atomically dispersed copper catalyst via CO-insertion**. *Materials Today Physics* 2021, **19**, 100418.

90. Lum Y, Cheng T, Goddard III WA, Ager JW: **Electrochemical CO reduction builds solvent water into oxygenate products**. *J Am Chem Soc* 2018, **140**:9337–9340.

91. Greenzaid P, Luz Z, Samuel D: **A nuclear magnetic resonance study of the reversible hydration of aliphatic aldehydes and ketones. II. The acid-catalyzed oxygen exchange of acetaldehyde**. *J Am Chem Soc* 1967, **89**:756–759.

92. Handoko AD, Chan KW, Yeo BS: **-CH_3 mediated pathway for the electroreduction of CO_2 to ethane and ethanol on thick oxide-derived copper catalysts at low overpotentials**. *ACS Energy Lett* 2017, **2**:2103–2109.

93. Zheng Y, Vasileff A, Zhou XL, Jiao Y, Jaroniec M, Qiao SZ: **Understanding the roadmap for electrochemical reduction of CO_2 to multi-carbon oxygenates and hydrocarbons on copper-based catalysts**. *J Am Chem Soc* 2019, **141**: 7646–7659.

94. Fan L, Xia C, Yang FQ, Wang J, Wang HT, Lu YY: **Strategies in catalysts and electrolyzer design for electrochemical CO_2 reduction toward C_{2+} products**. *Sci Adv* 2020, **6**. eaay 3111.

95. Li J, Wang Z, McCallum C, Xu Y, Li F, Wang Y, Gabardo CM, Dinh C-T, Zhuang T-T, Wang L, *et al.*: **Constraining CO coverage on copper promotes high-efficiency ethylene electroproduction**. *Nat Catal* 2019, **2**:1124–1131.

96. Li J, Chang K, Zhang H, He M, Goddard WA, Chen JG, Cheng M-J, Lu Q: **Effectively increased efficiency for electroreduction of carbon monoxide using supported polycrystalline copper powder electrocatalysts**. *ACS Catal* 2019, **9**:4709–4718.

97. Schröder D, Goldberg N, Zummack W, Schwarz H, Poutsma JC, Squires RR: **Generation of α-acetolactone and the acetoxyl diradical $\bullet CH_2COO\bullet$ in the gas phase**. *Int J Mass Spectrom Ion Process* 1997, **165–166**:71–82.

98. Ma M, Deng W, Xu A, Hochfilzer D, Qiao Y, Chan K, Chorkendorff I, Seger B: **Local reaction environment for selective electroreduction of carbon monoxide**. *Energy Environ Sci* 2022, **15**:2470–2478.

99. Shen H, Wang Y, Chakraborty T, Zhou G, Wang C, Fu X, Wang Y, Zhang J, Li C, Xu F, *et al.*: **Asymmetrical C-C coupling for electroreduction of CO on bimetallic Cu-Pd catalysts**. *ACS Catal* 2022, **12**:5275–5283.

100. Raciti D, Cao L, Livi KJT, Rottmann PF, Tang X, Li C, Hicks Z, Bowen KH, Hemker KJ, Mueller T, *et al.*: **Low-overpotential electroreduction of carbon monoxide using copper nanowires**. *ACS Catal* 2017, **7**:4467–4472.

101. Ren S, Zhang Z, Lees EW, Fink AG, Melo L, Hunt C, Dvorak DJ, Yu Wu W, Grant ER, Berlinguette CP: **Electrocatalysts derived from copper complexes transform CO into C_{2+} products effectively in a flow cell**. *Chem Eur J* 2022, **28**, e202200340.

102. Li S, Guan A, Yang C, Peng C, Lv X, Ji Y, Quan Y, Wang Q, Zhang L, Zheng G: **Dual-atomic Cu sites for electrocatalytic CO reduction to C_{2+} products**. *ACS Materials Letters* 2021, **3**: 1729–1737.

103. Luo M, Ozden A, Wang Z, Li F, Erick Huang J, Hung S-F, Wang Y, Li J, Nam D-H, Li YC, *et al.*: **Coordination polymer electrocatalysts enable efficient CO-to-Acetate conversion**. *Adv Mater* 2022, https://doi.org/10.1002/adma.202209567.

104. Verdaguer-Casadevall A, Li CW, Johansson TP, Scott SB, McKeown JT, Kumar M, Stephens IEL, Kanan MW, Chorkendorff I: **Probing the active surface sites for CO reduction on oxide-derived copper electrocatalysts**. *J Am Chem Soc* 2015, **137**:9808–9811.

105. Zhao YR, Chang XZ, Malkani AS, Yang X, Thompson L, Jiao F, Xu BJ: **Speciation of Cu surfaces during the electrochemical CO reduction reaction**. *J Am Chem Soc* 2020, **142**:9735–9743.

106. Zhai Y, Han P, Yun Q, Ge Y, Zhang X, Chen Y, Zhang H: **Phase engineering of metal nanocatalysts for electrochemical CO_2 reduction**. *eScience* 2022, **2**:467–485.

107. De Gregorio GL, Burdyny T, Loiudice A, Iyengar P, Smith WA, Buonsanti R: **Facet-dependent selectivity of Cu catalysts in electrochemical CO_2 reduction at commercially viable current densities**. *ACS Catal* 2020, **10**:4854–4862.

108. Hahn C, Hatsukade T, Kim Y-G, Vailionis A, Baricuatro JH, Higgins DC, Nitopi SA, Soriaga MP, Jaramillo TF: **Engineering Cu surfaces for the electrocatalytic conversion of CO_2: controlling selectivity toward oxygenates and hydrocarbons**. *Proc Nat Acad Sci USA* 2017, **114**:5918–5923.

109. Heenen HH, Shin H, Kastlunger G, Overa S, Gauthier JA, Jiao F, Chan K: **The mechanism for acetate formation in electrochemical CO_2 reduction on Cu: selectivity with potential, pH, and nanostructuring**. *Energy Environ Sci* 2022, **15**:3978–3990.

110. ** Wei P, Gao D, Liu T, Li H, Sang J, Wang C, Cai R, Wang G, Bao X: **Coverage-driven selectivity switch from ethylene to acetate in high-rate CO_2/CO electrolysis**. *Nat Nanotechnol* 2023, https://doi.org/10.1038/s41565-022-01286-y.

This work studied the effect of elevated pressure when using CO_2/CO feed and pure feed. This work revealed the CO converage enhancement and CO adsorption sites change would improve acetate selectivity. It achieves unprecedented acetate rate of 2.97 g min^{-1} at 250 A in high pressure CO feedstock.

111. Gunathunge CM, Li J, Li X, Hong JJ, Waegele MM: **Revealing the predominant surface facets of rough Cu electrodes under electrochemical conditions**. *ACS Catal* 2020, **10**:6908–6923.

112. Fan L, Xia C, Zhu P, Lu Y, Wang H: **Electrochemical CO_2 reduction to high-concentration pure formic acid solutions in an all-solid-state reactor**. *Nat Commun* 2020, **11**:3633.

113. Xia C, Zhu P, Jiang Q, Pan Y, Liang W, Stavitski E, Alshareef HN, Wang H: **Continuous production of pure liquid fuel solutions via electrocatalytic CO_2 reduction using solid-electrolyte devices**. *Nat Energy* 2019, **4**:776–785.

114. Leow WR, Lum Y, Ozden A, Wang Y, Nam D-H, Chen B, Wicks J, Zhuang T-T, Li F, Sinton D, *et al.*: **Chloride-mediated selective electrosynthesis of ethylene and propylene oxides at high current density**. *Science* 2020, **368**:1228–1233.

115. Li J, Wang Z, McCallum C, Xu Y, Li F, Wang Y, Gabardo CM, Cao-Thang D, Zhuang T-T, Wang L, *et al.*: **Constraining CO coverage on copper promotes high-efficiency ethylene electroproduction**. *Nat Catal* 2019, **2**:1124–1131.

116. Wang X, de Araujo JF, Ju W, Bagger A, Schmies H, Kuhl S, Rossmeisl J, Strasser P: **Mechanistic reaction pathways of enhanced ethylene yields during electroreduction of CO_2-CO co-feeds on Cu and Cu-tandem electrocatalysts**. *Nat Nanotechnol* 2019, **14**:1063–1070.

117. Zhou Y, Ganganahalli R, Verma S, Tan HR, Yeo BS: **Production of C_3-C_6 acetate esters via CO electroreduction in a membrane electrode assembly cell**. *Angewandte Chemie-International Edition* 2022, **61**, e202202859.

118. Hann EC, Overa S, Harland-Dunaway M, Narvaez AF, Le DN, Orozco-Cardenas ML, Jiao F, Jinkerson RE: **A hybrid inorganic-biological artificial photosynthesis system for energy-efficient food production**. *Nature Food* 2022, **3**:461–471.

119. Liu Z, Wang K, Chen Y, Tan T, Nielsen J: **Third-generation biorefineries as the means to produce fuels and chemicals from CO2**. *Nat Catal* 2020, **3**:274–288.